TABLE 1

Oligonucleotides used for the production of promoter constructs, site-directed mutagenesis, EMSA, and quantitative PCR

With regard to the oligonucleotides used for EMSA and site-directed mutagenesis, the HNF1-motif in the hOAT1 promoter is underlined. Boldface type indicates the difference in the sequence of the per and mut compared with the wild-type sequence found in the hOAT1 promoter.

Oligonucleotide	Orientation	Sequence (5′ to 3′)
Primers and oligonucleotides used for the cloning of 5′-flanking regions		
hOAT1		
−919	Forward	GGTACCTAATCACTTGAACCTGGGAGGC
−623	Forward	GGTACCCACCCGACATTGTGTATGACG
−318	Forward	GGTACCCCTGGCAACCCTTCCCAAAAGC
−111	Forward	GGTACCCCTGCCCTTTATAACCACTTGG
+11	Reverse	AAGCTTGGGCAGTTTTTAATCCTTGGCC
mOat1		
−110	Forward	GGTACCTTGCCCTTCATTCCCAATTGG
+10	Reverse	AAGCTTGGCAGCGTTTAATCTTTGTCC
Oligonucleotides used for the site-directed mutagenesis		
Mut	Sense	GGAATCCTTGGAGGG**GGCGATCCGTCTG**ATACCAAGTCAC
Oligonucleotides used for the construction of EMSA probe and competitor		
wt	Sense	TCCTTGGAGG**GTTAATCCTTCTG**ATACCAAGTC
Per	Sense	TCCTTGGAGG**GTTAATCATTAAC**ATACCAAGTC
Mut	Sense	TCCTTGGAGG**GGCGATCCGTCTG**ATACCAAGTC
Primers used for the quantitative PCR		
mOat1	Forward	GGCACCTTGATTGGCTATGT
	Reverse	AGCTTAGCCCCCTCTTCTTG
Mouse GAPDH	Forward	AACGACCCCTTCATTGAC
	Reverse	TCCACGACATACTCAGCAC

HindIII, yielding the hOAT1_−919/+11_HNF1wt and mOat1_−110/+10_HNF1wt promoter-reporter construct. A series of hOAT1 5′-truncated promoter fragments (−623/+11, −318/+11, and −111/+11) were PCR-amplified using hOAT1_−919/+11_HNF1wt plasmid as a template (the primers are shown in Table 1) and then inserted into the pGL3-Basic vector as described above, yielding the following promoter constructs: hOAT1_−623/+11_HNF1wt, −318/+11_HNF1wt, and −111/+11_HNF1wt. The sequence identity of all the constructs with the respective genomic sequences was verified by DNA sequencing. Plasmid DNA was prepared using the GenElute Plasmid Midiprep kit (Sigma-Aldrich, St. Louis, MO).

Site-Directed Mutagenesis. All of the mutated promoter fragments (HNF1mut) having a 4-bp-disrupted HNF1-motif were generated with a QuikChange XL Site-Directed Mutagenesis Kit (Stratagene, La Jolla, CA) using internally mutated oligonucleotides with sense sequence (as shown in Table 1) according to the manufacturer's instructions. The introduction of mutations was verified by DNA sequencing. The positions and bases that will replace the original sequences were decided based on the information in the database of transcription factors TRANSFAC (http://www.gene-regulation.com/); highly conserved bases in the consensus HNF1-motif were mutated into bases with the lowest frequency at the corresponding position.

Cell Culture, Transfections, and Luciferase Assays. Cell culture and transfections were performed as described previously. In transactivation assays, 0.5 μg of empty pcDNA3.1$^+$ control vector, 0.5 μg of HNF1α expression vector, 0.25 μg of HNF1α and HNF1β expression vectors, or 0.5 μg of HNF1β expression vector was cotransfected with 0.5 μg of the corresponding promoter construct and 0.05 μg of internal standard pRL-SV40 into HEK293 cells. The promoter activity was measured as relative light units of firefly luciferase per unit of *Renilla* luciferase. The difference in the promoter activity between wild-type and HNF1-mutated reporter constructs was statistically analyzed by the Student's *t* test.

In Vitro Translation. In vitro translation was performed using TNT Quick Coupled Transcription/Translation kits (Promega) according to the manufacturer's instructions. One microgram of empty pcDNA3.1$^+$ control vector, 1 μg of HNF1α expression vector, 0.5 μg of HNF1α and HNF1β expression vectors, or 1 μg of HNF1β expression vector was added to the TNT Quick master mix. The mixture was then incubated at 30°C for 75 min and used for additional analyses. The HNF1α and HNF1β proteins were prepared at least twice, and the reproducible binding to the labeled OAT1 probe was confirmed.

Electrophoretic Mobility Shift Assay. Double-stranded oligonucleotide probes were generated by hybridizing single-stranded complementary oligonucleotides with sense sequences (shown in Table 1). The sequence "wt" corresponds to the wild-type HNF1-motif found in the hOAT1 promoter, and "per" corresponds to the perfect consensus sequence for the HNF1-motif, whereas "mut" denotes the wild-type sequence mutated in the motif. Electrophoretic mobility shift assay (EMSA) was performed as previously described with Dig Gel Shift Kit, 2nd Generation (Roche Diagnostics, Indianapolis, IN) (Kikuchi et al., 2006). In brief, 2.5 μl of in vitro-translated HNF1α and/or HNF1β was incubated on ice for 30 min in the binding solution containing 0.92 pmol of digoxigenin-labeled probe. A 100-fold excess of unlabeled oligonucleotides and 1 μg of antibody against HNF1α or HNF1β (Santa Cruz Biotechnology, Inc., Santa Cruz, CA) were added to the reaction for competition and supershift assays, respectively. The experiments were independently performed three times, and the representative images are shown.

Results

Computational Analysis of the Potential Transcription Factor Binding Sites in Human and Mouse OAT1 Promoters. The promoter sequences of the human and mouse *OAT1* genes were obtained from the National Center for Biotechnology Information genome database and aligned using Genetyx-win version 8 software (Fig. 1). The promoter region of OAT1 was highly conserved between human and mouse, especially up to approximately 100 bp upstream of the transcriptional start site. Computational analysis using MatInspector revealed that the HNF1-motif is conserved at −56 to −44 relative to the transcriptional start site in both promoters, indicating the functional importance of this motif. Analysis using NUBIScan demonstrated that the IR-8 element was located at −123 to −104 in the hOAT1 promoter,

but not in the mOat1 promoter, suggesting the possible existence of a species difference in the regulation of OAT1 expression.

Impaired Expression of mOat1 in the Kidney of Hnf1α-Null Mice. The mRNA expression of mOat1 in male and female Hnf1α-null mice was measured by real-time quantitative PCR (Fig. 2). The expression of mOat1 mRNA was approximately 3-fold higher in male kidney than in female in wild-type controls, which is consistent with the previous findings (Buist and Klaassen, 2004). Inactivation of HNF1α led to a significant reduction in the expression of mOat1 in male mice. In females, the expression of mOat1 mRNA was reduced by two-thirds in Hnf1α-null mice compared with wild-type mice. These results clearly document the importance of HNF1α in the transcriptional regulation of the *mOat1* gene in the kidney.

Transactivation of the Human and Mouse OAT1 Promoter by HNF1α/β. We have previously demonstrated that endogenous expression of HNF1α and HNF1β is negligible in HEK293 cells (Kikuchi et al., 2006). Thus, this cell line was used in additional studies to investigate the effect of exogenously expressed HNF1α and/or HNF1β on *OAT1* gene promoter activity. The protein expression of exogenously transfected HNF1α or HNF1β in HEK293 cells was confirmed by Western blot analysis after preparation of nuclear extracts from those cells (data not shown). The promoter activity of mOat1 was stimulated by cotransfection of HNF1α alone or both HNF1α and HNF1β, whereas HNF1β alone did not show any enhancement (Fig. 3A). These results provide mechanistic evidence for the involvement of HNF1α in the transcription of mOat1 in the kidney.

To investigate whether HNF1α and/or HNF1β regulate hOAT1-promoter activity, a series of 5′-truncated-promoter constructs of hOAT1, with or without the mutation in the HNF1-motif, was cotransfected with HNF1α and/or HNF1β into HEK293 cells, and the luciferase activity was measured (Fig. 3B). All of the wild-type promoter constructs showed a marked increase in luciferase activity by forced-expression of HNF1α alone or both HNF1α and HNF1β compared with the pcDNA3.1$^+$-transfected control. The effect of HNF1β on the promoter activity of hOAT1 was not marked, regardless of the length of the promoter construct. No additional enhancement was observed by extending the hOAT1 promoter from −111 to −919, suggesting that HNF1α/β binds to the hOAT1-promoter region within 111 bp upstream of the transcriptional start site, where the HNF1-motif was found. The functional relevance of this HNF1-motif was investigated by introducing mutations into the motif. The increase in the luciferase activity caused by the forced expression of HNF1α alone or both HNF1α and HNF1β was attenuated by approximately 50 to 70% in the HNF1-motif-mutated reporter compared with the wild-type reporter. These results strongly suggest that the HNF1-motif found in the hOAT1-proximal promoter is essential for transactivation of the promoter activity by HNF1α alone or both HNF1α and HNF1β.

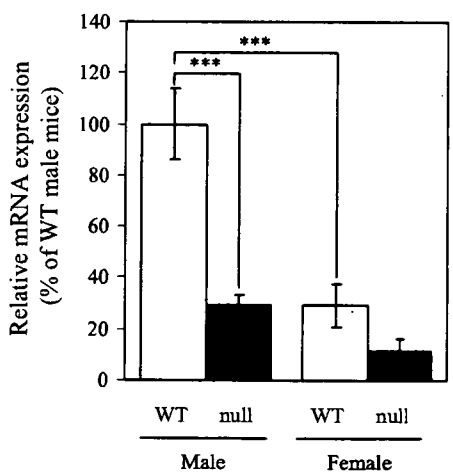

Fig. 2. Relative mRNA expression of mOat1 in wild-type and Hnf1α-null mice. mRNA expression of mOat1 in the kidneys of male or female wild-type (WT, □) and Hnf1α-null mice (null, ■) was quantified as described under *Materials and Methods*. The data were normalized by the mRNA expression of GAPDH. The relative mRNA expression was given as a ratio with respect to the mRNA expression of mOat1 in male wild-type mice that was taken as 100%. Results are presented as the mean ± S.E. of three (male) or four (female) mice. ***, $P < 0.001$, significantly different between the indicated data points.

Direct Binding of HNF1α/β to the hOAT1 Promoter. To confirm the direct binding of HNF1α/β to the hOAT1 promoter, EMSA was performed with the oligonucleotide probe corresponding to the HNF1-motif found in the hOAT1 promoter and in vitro-translated HNF1α and/or HNF1β (Fig. 4A). The expression of in vitro-translated HNF1α or HNF1β was confirmed by Western blot analysis with specific antibodies against HNF1α or HNF1β, respectively (data not shown). When the probe was incubated with HNF1α alone or both HNF1α and HNF1β, one- (Fig. 4A, band *a*, lane 3) or two-shifted bands (Fig. 4A, bands *a* and *b*, lane 7) were observed, respectively, whereas there was no shifted band when the probe was incubated with HNF1β alone (lane 11). In all samples using the in vitro-translated products, a broad signal was detected below the bands (Fig. 4A, bands *a* and *b*). It is likely that this signal represents nonspecific binding to the labeled probe because the signal was also detected when in vitro-translated empty pcDNA3.1$^+$ was incubated with the probe (Fig. 4A, lane 2). Formation of both bands *a* and *b* (Fig. 4A) was completely abolished by adding a 100-fold excess of the unlabeled competitor corresponding to the consensus sequence for the HNF1-motif (Fig. 4A, lanes 4 and 8) and partly inhibited by the competitor corresponding to the hOAT1 wild-type promoter sequence (Fig. 4A, lanes 5 and 9). On the other hand, these bands were not affected by the addition of the mutated competitor (Fig. 4A, lanes 6 and 10). These results suggest that bands *a* and *b* (Fig. 4A) can be ascribed to the binding of HNF1α or HNF1β to the HNF1-motif in the hOAT1 promoter.

To demonstrate the specific binding of HNF1 to the hOAT1 promoter, supershift analysis was performed using antibodies against HNF1α or HNF1β (Fig. 4B). The addition of an anti-HNF1α antibody resulted in the supershift of both bands *a* and *b* (Fig. 4B, lanes 2 and 5), whereas the addition of anti-HNF1β antibody abolished band *b* but not band *a* (Fig. 4B, lanes 3 and 6). The supershifted bands were barely detectable when both HNF1α and HNF1β were incubated with the labeled probe (Fig. 4B, lanes 5 and 6), probably due to the low intensity of the shifted bands. The mobility of bands *a* and *b* (Fig. 4B) in the present study nearly coincides with that of the shifted bands that reflect the interaction of HNF1α/HNF1α homodimer and HNF1α/HNF1β heterodimer with the HNF1-motif in hOAT3 and human URAT1 promoters, respectively (Kikuchi et al., 2006, 2007). These results strongly suggest that bands *a* and *b* (Fig. 4B) reflect the

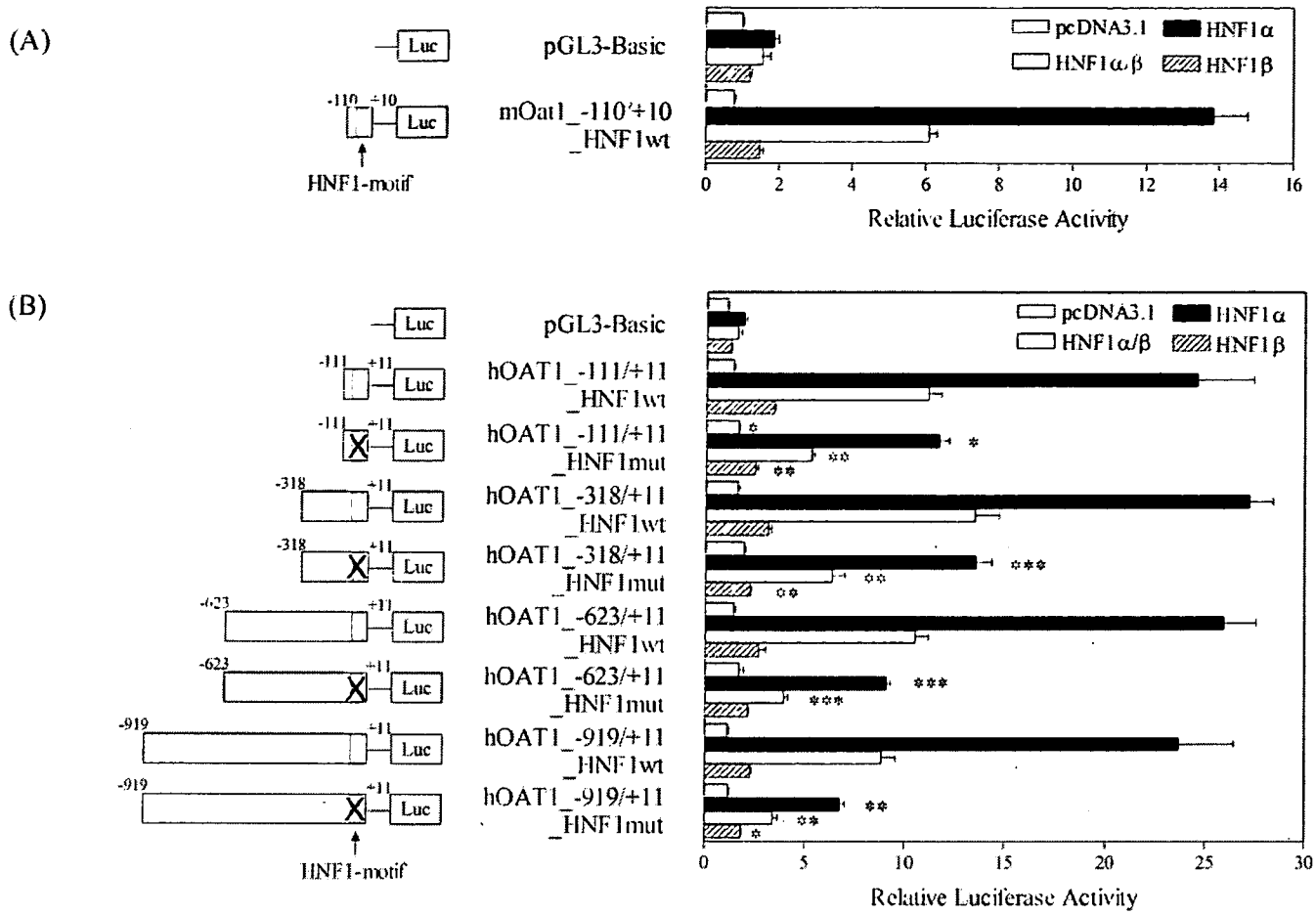

Fig. 3. Transactivation of human and mouse OAT1 promoters by HNF1α and/or HNF1β. A, HEK293 cells were transfected with mOat1 wild-type promoter (mOat1_−110/+10_HNF1wt), or a promoterless pGL3-Basic plasmid, together with empty pcDNA3.1$^+$ vector (white bars), HNF1α expression vector (black bars), HNF1α, and HNF1β expression vectors (gray bars), or HNF1β expression vector (hatched bars). The luciferase activity was measured as described under *Materials and Methods* and was shown as the factor of induction over background activity measured in cells transfected with pGL3-Basic together with pcDNA3.1$^+$. B, the activity of a series of hOAT1 wild-type or HNF1-mutated promoters in the presence or absence of exogenously expressed HNF1α and/or HNF1β was measured as described in A. Results are presented as the mean ± S.E. of triplicate samples. *, $P < 0.05$, **, $P < 0.01$, and ***, $P < 0.001$, significantly different between wild-type and the corresponding HNF1-mutated promoters.

binding of HNF1α/HNF1α homodimer and HNF1α/HNF1β heterodimer, respectively.

Discussion

Cumulative evidence suggests that HNF1α and/or HNF1β play a critical role in the expression of drug transporters in the liver and kidney. Several groups, including us, have shown that the HNF1-motif located within approximately 100 bp of the 5′-flanking region is involved in the transcriptional regulation of these transporters, i.e., −65 to −53 in the OAT3 promoters, −70 to −58 in the URAT1 promoters, −51 to −39 in the organic anion-transporting polypeptide 1B1 promoter, and −60 to −48 in the organic anion-transporting polypeptide 1B3 promoter (Jung et al., 2001; Kikuchi et al., 2006, 2007). Consistent with this finding, a database search for the potential transcription factor binding sites revealed that an HNF1-motif is conserved from −56 to −44 relative to the transcriptional start sites of the human and mouse OAT1 promoters (Fig. 1). These observations as well as the reduced expression of mOat1 in the kidney of Hnf1α-null male mice (Maher et al., 2006) prompted us to investigate the role of HNF1α/β in the transcriptional regulation of human and mouse *OAT1* genes.

The involvement of HNF1α and/or HNF1β in the transcriptional regulation of human and mouse *OAT1* genes was revealed by in vivo (Fig. 2) and in vitro experiments (Figs. 3 and 4). It is generally accepted that the transactivation potency of HNF1β is lower than that of HNF1α (Rey-Campos et al., 1991). Indeed, exogenous expression of HNF1β alone enhanced the promoter activity of OAT3 and URAT1 by at most 50% compared with that of HNF1α alone (Kikuchi et al., 2006, 2007). In the present study, HNF1β alone hardly stimulated the promoter activity of the human and mouse *OAT1* genes, and no direct binding of HNF1β/HNF1β homodimer to the hOAT1 promoter could be detected. HNF1β exhibited less activity against the OAT1 promoters than OAT3 and URAT1 promoters. Therefore, it is likely that the contribution of HNF1β/HNF1β homodimer to the expression of OAT1 is much smaller than that of OAT3 and URAT1.

Ogasawara et al. (2007) demonstrated that HNF4α markedly transactivated the hOAT1 promoter through direct binding to the IR-8 element, whereas neither HNF1α nor HNF1β affected the promoter activity. On the other hand, we

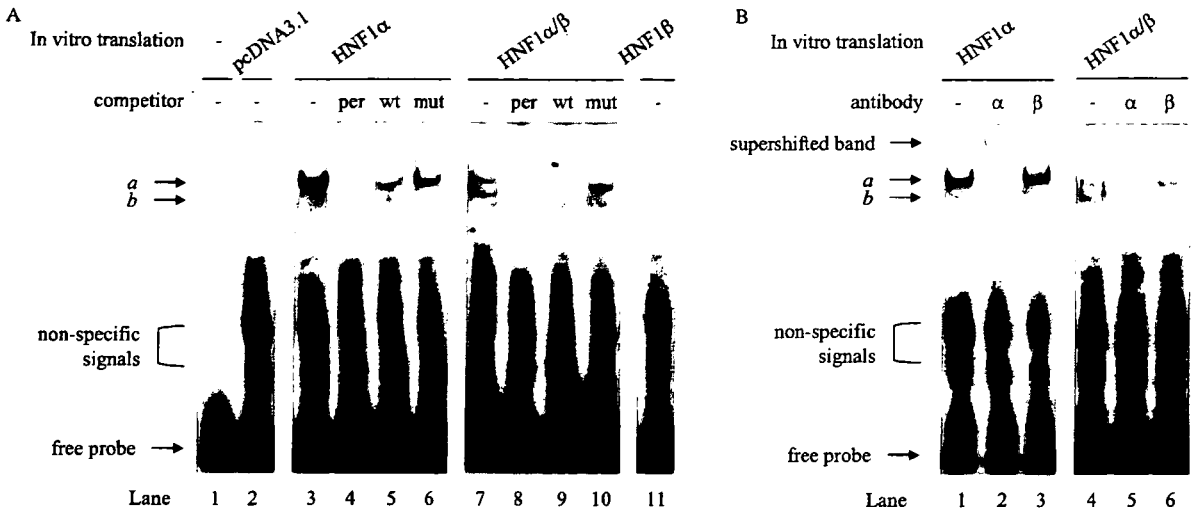

Fig. 4. Direct binding of HNF1α and HNF1β to the hOAT1 promoter. A, competition assays are shown. A digoxigenin-labeled probe corresponding to the hOAT1 wild-type promoter containing the HNF1-motif was incubated with in vitro-translated HNF1α and/or HNF1β, or pcDNA3.1$^+$ as a negative control, in the presence or absence of a 100-fold excess of unlabeled competitor (per, wt, or mut) as indicated. B, supershift analysis is shown. The probe was incubated with HNF1α alone or both HNF1α and HNF1β in the presence or absence of a specific antibody against HNF1α (α) or HNF1β (β) as indicated. The DNA-protein complex was detected as described under *Materials and Methods*. The representative images of three independent experiments are shown.

have provided clear evidence for an essential role of HNF1α in human and mouse OAT1 expression. We also confirmed that HNF4α transactivates the hOAT1 promoter. Cotransfection of HNF4α into HEK293 cells enhanced the promoter activity of the hOAT1_−919/+11_HNF1wt construct 3-fold compared with the pcDNA3.1$^+$-transfected control (data not shown). Therefore, the experimental conditions may not be appropriate for examining the effect of HNF1α/β in the previous report. The two studies used different cell lines as host. We used HEK293 cells that lack the endogenous expression of HNF1α/β, whereas Ogasawara et al. (2007) used OK cells in which the endogenous expression of HNF1α/β has not been investigated. The following difference in the reporter construct used could be another reason: hOAT1_−2747/+88 (Ogasawara et al., 2007) versus hOAT1_−919, −623, −318, or −111/+11_HNF1wt (present study).

In the kidney, the expression of both HNF1α and HNF4α is restricted to the proximal tubules (Lazzaro et al., 1992; Pontoglio et al., 1996; Jiang et al., 2003), consistent with the regional distribution of hOAT1 (Hosoyamada et al., 1999). Thus, the proximal tubule-specific expression of hOAT1 in the kidney is, at least partly, explained by the concerted effect of HNF1α/HNF1β heterodimer and HNF4α/HNF4α homodimer. However, the tissue distribution of HNF1αβ and HNF4α is much wider than that of OAT1 (Sladek et al., 1990; Blumenfeld et al., 1991; Rey-Campos et al., 1991; Miquerol et al., 1994; Drewes et al., 1996). Although OAT1 is exclusively expressed in the kidney, HNF1α, HNF1β, and HNF4α are expressed in extrarenal tissues, such as the liver, intestine, and pancreas. We have recently shown that the kidney-specific expression of *OAT3* and *URAT1* genes is regulated by the synergistic effect of transcriptional activation by HNF1α/β and repression by DNA methylation in the promoter region. However, unlike the minimal promoter regions of hOAT3 and human/mouse URAT1, there are few CpG dinucleotides in the human and mouse OAT1 promoter regions up to −400 bp (Fig. 1). It is noteworthy that *OAT1* and *OAT3* genes occur as a tightly linked pair on the same chromosome in the human and mouse genome with intergenic distances of 8.3 kilobase pairs in humans and 7.5 kilobase pairs in mice (Eraly et al., 2003). Both genes are transcribed to the same direction with OAT3 upstream of OAT1. The clustering of OAT1 and OAT3 in the genome raises the possibility that the methylation status of the OAT3 promoter region may affect the widespread chromatin configuration including the *OAT1* gene, enabling DNA methylation-dependent gene silencing of OAT1 in extrarenal tissues. Future studies are required to show the in vivo relevance of the epigenetic regulation for OAT1 expression.

In conclusion, the present study clearly demonstrates that HNF1α/HNF1β heterodimer plays a key role in the constitutive expression of human and mouse *OAT1* genes. The transcriptional activation by HNF1 is a common feature among renal organic anion transporters, further emphasizing the role of this transcription factor in the regulation of endobiotics/xenobiotics transport in the kidney.

References

Blumenfeld M, Maury M, Chouard T, Yaniv M, and Condamine H (1991) Hepatic nuclear factor 1 (HNF1) shows a wider distribution than products of its known target genes in developing mouse. *Development* **113**:589–599.

Buist SC and Klaassen CD (2004) Rat and mouse differences in gender-predominant expression of organic anion transporter (Oat1–3; Slc22a6–8) mRNA levels. *Drug Metab Dispos* **32**:620–625.

Chen WS, Manova K, Weinstein DC, Duncan SA, Plump AS, Prezioso VR, Bachvarova RF, and Darnell JE Jr (1994) Disruption of the HNF-4 gene, expressed in visceral endoderm, leads to cell death in embryonic ectoderm and impaired gastrulation of mouse embryos. *Genes Dev* **8**:2466–2477.

Cihlar T, Ho ES, Lin DC, and Mulato AS (2001) Human renal organic anion transporter 1 (hOAT1) and its role in the nephrotoxicity of antiviral nucleotide analogs. *Nucleosides Nucleotides Nucleic Acids* **20**:641–648.

Drewes T, Senkel S, Holewa B, and Ryffel GU (1996) Human hepatocyte nuclear factor 4 isoforms are encoded by distinct and differentially expressed genes. *Mol Cell Biol* **16**:925–931.

Enomoto A and Endou H (2005) Roles of organic anion transporters (OATs) and a urate transporter (URAT1) in the pathophysiology of human disease. *Clin Exp Nephrol* **9**:195–205.

Eraly SA, Hamilton BA, and Nigam SK (2003) Organic anion and cation transporters occur in pairs of similar and similarly expressed genes. *Biochem Biophys Res Commun* **300**:333–342.

Eraly SA, Vallon V, Vaughn DA, Gangoiti JA, Richter K, Nagle M, Monte JC, Rieg T, Truong DM, Long JM, et al. (2006) Decreased renal organic anion secretion and plasma accumulation of endogenous organic anions in OAT1 knock-out mice. *J Biol Chem* **281**:5072–5083.

Fraser JD, Martinez V, Straney R, and Briggs MR (1998) DNA binding and transcription activation specificity of hepatocyte nuclear factor 4. *Nucleic Acids Res* **26**:2702–2707.

Gresh L, Fischer E, Reimann A, Tanguy M, Garbay S, Shao X, Hiesberger T, Fiette L, Igarashi P, Yaniv M, et al. (2004) A transcriptional network in polycystic kidney disease. *EMBO J* **23**:1657–1668.

Ho ES, Lin DC, Mendel DB, and Cihlar T (2000) Cytotoxicity of antiviral nucleotides adefovir and cidofovir is induced by the expression of human renal organic anion transporter 1. *J Am Soc Nephrol* **11**:383–393.

Hosoyamada M, Sekine T, Kanai Y, and Endou H (1999) Molecular cloning and functional expression of a multispecific organic anion transporter from human kidney. *Am J Physiol* **276**:F122–F128.

Jiang S, Tanaka T, Iwanari H, Hotta H, Yamashita H, Kumakura J, Watanabe Y, Uchiyama Y, Aburatani H, Hamakubo T, et al. (2003) Expression and localization of P1 promoter-driven hepatocyte nuclear factor-4α (HNF4α) isoforms in human and rats. *Nucl Recept* **1**:5.

Jung D, Hagenbuch B, Gresh L, Pontoglio M, Meier PJ, and Kullak-Ublick GA (2001) Characterization of the human OATP-C (SLC21A6) gene promoter and regulation of liver-specific OATP genes by hepatocyte nuclear factor 1α. *J Biol Chem* **276**: 37206–37214.

Kikuchi R, Kusuhara H, Hattori N, Kim I, Shiota K, Gonzalez FJ, and Sugiyama Y (2007) Regulation of tissue-specific expression of the human and mouse urate transporter 1 gene by hepatocyte nuclear factor 1αβ and DNA methylation. *Mol Pharmacol* **72**:1619–1625.

Kikuchi R, Kusuhara H, Hattori N, Shiota K, Kim I, Gonzalez FJ, and Sugiyama Y (2006) Regulation of the expression of human organic anion transporter 3 by hepatocyte nuclear factor 1αβ and DNA methylation. *Mol Pharmacol* **70**:887–896.

Lazzaro D, De Simone V, De Magistris L, Lehtonen E, and Cortese R (1992) LFB1 and LFB3 homeoproteins are sequentially expressed during kidney development. *Development* **114**:469–479.

Lee YH, Sauer B, and Gonzalez FJ (1998) Laron dwarfism and non-insulin-dependent diabetes mellitus in the Hnf-1α knockout mouse. *Mol Cell Biol* **18**: 3059–3068.

Maher JM, Slitt AL, Callaghan TN, Cheng X, Cheung C, Gonzalez FJ, and Klaassen CD (2006) Alterations in transporter expression in liver, kidney, and duodenum after targeted disruption of the transcription factor HNF1α. *Biochem Pharmacol* **72**:512–522.

Mendel DB and Crabtree GR (1991) HNF-1, a member of a novel class of dimerizing homeodomain proteins. *J Biol Chem* **266**:677–680.

Miquerol L, Lopez S, Cartier N, Tulliez M, Raymondjean M, and Kahn A (1994) Expression of the L-type pyruvate kinase gene and the hepatocyte nuclear factor 4 transcription factor in exocrine and endocrine pancreas. *J Biol Chem* **269**:8944–8951.

Ogasawara K, Terada T, Asaka J, Katsura T, and Inui K (2007) Hepatocyte nuclear factor-4α regulates the human organic anion transporter 1 gene in the kidney. *Am J Physiol Renal Physiol* **292**:F1819–F1826.

Podvinec M, Kaufmann MR, Handschin C, and Meyer UA (2002) NUBIScan, an in silico approach for prediction of nuclear receptor response elements. *Mol Endocrinol* **16**:1269–1279.

Pontoglio M, Barra J, Hadchouel M, Doyen A, Kress C, Bach JP, Babinet C, and Yaniv M (1996) Hepatocyte nuclear factor 1 inactivation results in hepatic dysfunction, phenylketonuria, and renal Fanconi syndrome. *Cell* **84**:575–585.

Popowski K, Eloranta JJ, Saborowski M, Fried M, Meier PJ, and Kullak-Ublick GA (2005) The human organic anion transporter 2 gene is transactivated by hepatocyte nuclear factor-4α and suppressed by bile acids. *Mol Pharmacol* **67**:1629–1638.

Prieur X, Schaap FG, Coste H, and Rodriguez JC (2005) Hepatocyte nuclear factor-4α regulates the human apolipoprotein AV gene: identification of a novel response element and involvement in the control by peroxisome proliferator-activated receptor-γ coactivator-1α, AMP-activated protein kinase, and mitogen-activated protein kinase pathway. *Mol Endocrinol* **19**:3107–3125.

Rey-Campos J, Chouard T, Yaniv M, and Cereghini S (1991) vHNF1 is a homeoprotein that activates transcription and forms heterodimers with HNF1. *EMBO J* **10**:1445–1457.

Saborowski M, Kullak-Ublick GA, and Eloranta JJ (2006) The human organic cation transporter-1 gene is transactivated by hepatocyte nuclear factor-4α. *J Pharmacol Exp Ther* **317**:778–785.

Sekine T, Miyazaki H, and Endou H (2006) Molecular physiology of renal organic anion transporters. *Am J Physiol Renal Physiol* **290**:F251–F261.

Shih DQ, Bussen M, Sehayek E, Ananthanarayanan M, Shneider BL, Suchy FJ, Shefer S, Bollileni JS, Gonzalez FJ, Breslow JL, et al. (2001) Hepatocyte nuclear factor-1α is an essential regulator of bile acid and plasma cholesterol metabolism. *Nat Genet* **27**:375–382.

Sladek FM, Zhong WM, Lai E, and Darnell JE Jr (1990) Liver-enriched transcription factor HNF-4 is a novel member of the steroid hormone receptor superfamily. *Genes Dev* **4**:2353–2365.

Sweet DH, Miller DS, Pritchard JB, Fujiwara Y, Beier DR, and Nigam SK (2002) Impaired organic anion transport in kidney and choroid plexus of organic anion transporter 3 (*Oat3* (*Slc22a8*)) knockout mice. *J Biol Chem* **277**:26934–26943.

Tronche F and Yaniv M (1992) HNF1, a homeoprotein member of the hepatic transcription regulatory network. *Bioessays* **14**:579–587.

Address correspondence to: Dr. Yuichi Sugiyama, Department of Molecular Pharmacokinetics, Graduate School of Pharmaceutical Sciences, The University of Tokyo, 7-3-1 Hongo, Bunkyo-ku, Tokyo 113-0033. E-mail: sugiyama@mol.f.u-tokyo.ac.jp

0026-895X/07/7204-967-975$20.00
MOLECULAR PHARMACOLOGY
Copyright © 2007 The American Society for Pharmacology and Experimental Therapeutics
Mol Pharmacol 72:967-975, 2007

Vol. 72, No. 4
34751/3258864
Printed in U.S.A.

Effect of Breast Cancer Resistance Protein (Bcrp/*Abcg2*) on the Disposition of Phytoestrogens

Junichi Enokizono, Hiroyuki Kusuhara, and Yuichi Sugiyama

Graduate School of Pharmaceutical Sciences, the University of Tokyo, Tokyo, Japan

Received February 4, 2007; accepted July 20, 2007

ABSTRACT

The effect of breast cancer resistance protein (Bcrp/*Abcg2*) on the disposition of the phytoestrogens daidzein, genistein, and coumestrol was investigated using *Bcrp*$^{-/-}$ mice. Expression of the genes for either mouse Bcrp or human BCRP in MDCK II cells induced apically directed transport of the three phytoestrogens, whereas their transcellular transport was identical in mock and LLC-PK1 cells expressing mouse Mdr1a. After oral administration, the plasma levels of daidzein and genistein were increased in *Bcrp*$^{-/-}$ mice, but only a minimal change was observed for coumestrol. At steady state, tissue-to-plasma concentration ratios of the three phytoestrogens in the brain and testis of wild-type mice were very small and similar to those of [^{14}C]inulin, whereas those were significantly increased in the brain and testis of *Bcrp*$^{-/-}$ mice. The largest increases were observed with genistein (9.2- and 5.8-fold in the brain and testis, respectively). The distributions of genistein in the epididymis and fetus, but not the ovary, were also increased in *Bcrp*$^{-/-}$ mice. The Bcrp protein was localized in the luminal membrane of the endothelial cells in the testis and the body of the epididymis and in both the luminal and abluminal side of ducts in the head of the epididymis. These results suggest that Bcrp limits the oral availability and distribution into the brain and testis, epididymis, and fetus of phytoestrogens.

Phytoestrogens are plant compounds that produce estrogen-like activity in mammals. Daidzein and genistein are two major isoflavonoids included in soy-based food and are the most commonly consumed phytoestrogens. Coumestrol, an isoflavone present in high concentrations in red clover, is known as the most potent estrogen among phytoestrogens (Mueller et al., 2004). Because of their estrogenic activity, phytoestrogens have been proposed as alternative agents for the treatment of postmenopausal disease; this concept has been supported by some clinical studies (Cassidy et al., 1995; Watanabe et al., 2000). Furthermore, epidemiological studies suggest that the low incidences of prostate, breast, and colon cancers and coronary disease in Asian populations are associated with the high consumption of isoflavonoids, a group of phytoestrogens highly included in soy-based diets (Adlercreutz, 1995). Based on these findings, phytoestrogens are believed to be beneficial for human health and are widely consumed in food and food supplements. On the other hand, warnings against the excessive consumption of phytoestrogens have been issued, because some adverse effects of phytoestrogens have been reported. For example, perinatal and neonatal exposure to genistein caused abnormalities in the ovary and vagina, reduced size of the testis and prostate, and caused the suppression of sexual behavior in rodents (Delclos et al., 2001; Wisniewski et al., 2003; Kyselova et al., 2004). Suppressive effects on sexual behavior were also reported for coumestrol in rats (Whitten et al., 2002).

The disposition of phytoestrogens has been well studied for genistein and daidzein. These exist naturally in the glycoside forms. Upon ingestion, they are hydrolyzed by bacterial β-glycosidase and are absorbed mainly as an aglycon (Setchell et al., 2002). Genistein and daidzein are predominantly metabolized to the glucuronide conjugates in the intestine and liver, followed by excretion into the bile (Chen et al., 2005). In the intestinal lumen, the glucuronide conjugates are hydrolyzed by bacterial β-glucuronidase and reabsorbed (Sfakianos et al., 1997). Thus, both genistein and daidzein undergo enterohepatic circulation. Tissue and fetal distributions of genistein have been investigated in rats (Chang et al., 2000; Doerge et al., 2001). Very low distributions of

This work was supported by a Health and Labour Sciences Research Grant from Ministry of Health, Labour and Welfare for the Research on Advanced Medical Technology (to Y.S.), and by a grant-in-aid for scientific research (B) from Japan Society for the Promotion of Science (KAKENHI 18390046 to H.K.).
Article, publication date, and citation information can be found at http://molpharm.aspetjournals.org.
doi:10.1124/mol.107.034751.

ABBREVIATIONS: Bcrp, breast cancer resistance protein; mBcrp, mouse breast cancer resistance protein, hBCRP; human breast cancer resistance protein; GFP, green fluorescent protein; L-Mdr1a, LLC-PK1 cells expressing mouse Mdr1a; AUC, area under the curve; K_p, tissue-to-plasma concentration ratio; PCR, polymerase chain reaction; BSA, bovine serum albumin; PBS, phosphate-buffered saline; LC, liquid chromatography.

genistein were observed in the brain and testis, whereas moderate and high distributions were found in the other hormone target organs (prostate, ovary, and uterus) (Chang et al., 2000). Furthermore, in pregnant rats exposed to genistein, serum genistein concentrations were approximately 5 times less in fetuses than in maternal rats (Doerge et al., 2001). These findings suggest that penetration of genistein into the brain, testis, and fetus are limited by the blood-brain, -testis, and -placental barriers, attenuating the toxicological effects of genistein on the development of the brain, testis, and fetus.

Here we investigated the role of the breast cancer resistance protein (Bcrp/*Abcg2*) in the disposition of phytoestrogens. Bcrp is a member of the ATP-binding cassette transporter family and mediates the efflux transport of endo- and xenobiotics. Bcrp is expressed in various normal tissues (Maliepaard et al., 2001), and cumulative in vivo studies, particularly using *Bcrp*$^{-/-}$ mice, revealed important roles for this protein in the site of absorption and in clearance organs (van Herwaarden et al., 2003; Breedveld et al., 2004; Mizuno et al., 2004; Hirano et al., 2005). In addition, BCRP is also expressed in various tissue barriers, such as those in the brain, testis, and placenta (Jonker et al., 2002; Zhang et al., 2003; Bart et al., 2004). In these tissue barriers, Bcrp is expressed in the plasma membranes facing circulating blood and has its protective role against xenobiotics. Indeed, it was shown using *Bcrp*$^{-/-}$ mice that Bcrp restricts the penetration of imatinib and topotecan into the brain and fetus, respectively (Jonker et al., 2002; Breedveld et al., 2005). As far as phytoestrogens are concerned, many of them can interact with human BCRP at least as inhibitors, but genistein was found to be a BCRP substrate (Imai et al., 2004). Here, we compared the plasma concentration time profiles and tissue distribution of phytoestrogens (daidzein, genistein, and coumestrol) in the brain, testis, epididymis, and fetus using *Bcrp*$^{-/-}$ mice. We found that Bcrp limited the oral availability and penetration into the brain, testis, and epididymis of genistein and the penetration of daidzein and coumestrol into the brain and testis.

Materials and Methods

Materials and Animals

Daidzein, genistein, and coumestrol were purchased from Sigma-Aldrich (St. Louis, MO), and ^{14}C-labeled inulin was from Moravek Biochemicals (Brea, CA). All of the other chemicals were commercially available and of reagent grade. Wild-type FVB mice and *Bcrp*$^{-/-}$ mice (Jonker et al., 2002) were used in the present study. Male mice (9–17 weeks old and 23–32 g body weight) were used in the studies of oral administration and tissue distribution (brain, testis, and epididymis). Female mice (15–16 weeks old and 24–28 g body weight) were used in the ovary distribution study. Pregnant female mice used in the fetus distribution study were at 2 weeks' gestation and weighed 35 to 48 g. All of these animals were maintained under controlled temperature with a light/dark cycle. Food and water were available ad libitum except for the oral administration study in which mice were fasted for approximately 12 h before administration.

Transcellular Transport Study

The transcellular transport study was performed as reported previously with minor modifications (Matsushima et al., 2005). In brief, MDCK II cells were seeded in the 24-well Transwell (Corning, Cambridge, MA) at a density of 1.4×10^5 cells/well and grown for 3 days in Dulbecco's modified Eagle's medium (Invitrogen, Carlsbad, CA) with 10% fetal bovine serum (Sigma-Aldrich) and 1% antibiotic-antimycotic solution (Sigma-Aldrich). The cells were infected with the recombinant adenovirus harboring expression vector for green fluorescent protein (GFP), mouse Bcrp (mBcrp) or human BCRP (hBCRP) at 200 multiplicity of infection. The details of the construction of these recombinant adenoviruses were described in a previous report (Kondo et al., 2004). After 2 days of culture, the cells were used for transport studies. The cells were preincubated in Krebs-Henseleit buffer (142 mM NaCl, 23.8 mM Na_2CO_3, 4.83 mM KCl, 0.96 mM KH_2PO_4, 1.20 mM $MgSO_4$, 12.5 mM HEPES, 5 mM glucose, and 1.53 mM $CaCl_2$, pH 7.4) at 37°C for 30 min, and transport experiments were initiated by replacing the medium on one side of the cell monolayer with Krebs-Henseleit buffer containing 3 μM test compounds. At appropriate times, 100-μl aliquots were taken from the opposite side of the cell monolayer and replaced with 100 μl of buffer.

In vitro transport by mMdr1a was examined using Mdr1a-expressing LLC-PK1 cells (L-Mdr1a). L-Mdr1a was established previously (Smith et al., 1998). L-Mdr1a and parent LLC-PK1 cells were seeded in the 24-well Transwell at a density of 4.8×10^5 cells/well and grown in medium 199 (Invitrogen) with 10% fetal bovine serum and 1% antibiotic-antimycotic solution. Medium was changed on the second day, and cells were subjected to the transport study on the fourth day. The procedures of the transport study were the same as those used for mBcrp and hBCRP. Efflux rates were calculated from the slopes of the time profiles of apical-to-basal and basal-to-apical transport. Flux ratios were obtained by dividing the efflux rates in the basal-to-apical direction by those in the apical-to-basal direction.

Animal Experiments

Oral Administration. Animals were fasted 12 h before administration. Compounds were suspended in 0.5% methylcellulose and orally administered at a dose of 30 μmol/kg. Blood was collected from tail vein at appropriate time points and was centrifuged at 4°C and 1000*g* for 5 min to obtain plasma.

Tissue and Fetus Distribution. Under urethane anesthesia (1.25 g/kg, i.p.), the right jugular vein was cannulated with a polyethylene tube (PE-50; BD Biosciences, San Jose, CA). Compounds were solubilized at a concentration of 1.25 mM in 10% dimethyl sulfoxide/90% saline containing 2 mM NaOH and continuously infused through the cannula at a dose rate of 5 μmol/h/kg. Blood was collected from the left jugular vein at 60, 80, 100, and 120 min and centrifuged at 4°C and 1000*g* for 5 min to obtain plasma. Immediately after the last blood sampling, mice were sacrificed by cervical dislocation, and tissues or fetus was collected. PBS was added to tissues or fetus and homogenized to make 20% homogenate for brain and testis, 10% homogenate for epididymis, 5% homogenate for ovary, and 33% homogenate for fetus. All of the samples were stored at −80°C until use.

[^{14}C]Inulin Distribution. Inulin cannot penetrate cellular membrane, therefore [^{14}C]inulin was used as a marker of space outside of barriers in the brain and testis. Under urethane anesthesia (1.25 g/kg, i.p.), [^{14}C]inulin was administered intravenously from the right jugular vein (50 μCi/kg). At 10-min postdose, blood was collected from the left jugular vein, and mice were sacrificed by cervical dislocation, and then the brain, testis, and epididymis were collected. Blood was centrifuged at 4°C and 1000*g* for 5 min, and plasma was obtained. Plasma (10 μl) was mixed with 8 ml of Hionic-Fluor (PerkinElmer Life and Analytical Sciences, Waltham, MA), and the radioactivity was measured with a liquid scintillation counter (LS 6000SE; Beckman Coulter, Fullerton, CA). Tissues were mixed with 400 μl of hydrogen peroxide and 800 μl of 2-propanol and left for 1 h at room temperature. Subsequently, 1 ml of Soluene 350 (PerkinElmer Life and Analytical Sciences) was added and incubated at 55°C for 4 h to solubilized the tissues. 10 ml of Hionic-Fluor was added and then subjected to a liquid scintillation counter (LS 6000SE).

LC/Mass Spectrometry Analysis

Samples were precipitated with two (for in vitro samples) or three (for in vivo samples) volumes of acetonitrile and centrifuged at 4°C and 15,000*g* for 10 min. After the evaporation of supernatants, the pellets were reconstituted with 10% acetonitrile/90% water and subjected to LC/mass spectrometry analysis. LCMS-2010 EV equipped with a Prominence LC system (Shimadzu, Kyoto, Japan) was used for the analysis. Samples were separated on a CAPCELL PAK C18 MGII column (3 μm, 2 × 50 mm; Shiseido, Tokyo, Japan) in a binary gradient mode. Mobile phase A was 0.05% formic acid, and mobile phase B was acetonitrile. For the analysis of daidzein and genistein, the concentration of mobile phase B was initially 18%, linearly increased up to 60% over 1.5 min, kept at 60% for a further 1 min, and finally re-equilibrated at 18% for 2.5 min. The total run time was 5 min. Daidzein and genistein were eluted at 3.0 and 3.3 min, respectively. For the analysis of coumestrol, the concentration of mobile phase B was initially 25%, linearly increased up to 90% over 1.5 min, kept at 90% for a further 1 min, and finally re-equilibrated at 25% for 3 min. Coumestrol was eluted at 2.7 min. Daidzein, genistein, and coumestrol were detected at mass-to-charge ratios of 255, 269, and 267, respectively, under negative electron-spray ionization mode. The interface voltage was −3.5 kV and the nebulizer gas (N_2) flow was 1.5 l/min. The heat block and curved desolvation line temperatures were 200 and 150°C, respectively.

Quantification of mRNA Level of BCRP in Mouse and Human Epididymis

Mice were anesthetized with ether and sacrificed by exsanguination from the femoral artery and vein. Immediately after sacrifice, the epididymis was collected. Total RNA was isolated from these tissues with using ISOGEN (Wako Pure Chemical Industries, Tokyo, Japan). Total RNA of human epididymis was purchased from BioChain Institute (Hayward, CA). Total RNA from mouse and human epididymis was converted to cDNA using random primer and avian myeloblastosis virus reverse transcriptase. Real-time PCR was performed with a QuantiTect SYBR Green PCR Kit (QIAGEN, Valencia, CA) and a LightCycler system (Roche Diagnostics, Mannheim, Germany). PCR primers were as follows: mouse Bcrp: forward, AAATGGAGCACCTCAACCTG; reverse, CCCATCACAACGTCATCTTG; human BCRP: forward, CAGGTCTGTTGGTCAATCTCACA; reverse, TCCATATCGTGGAATGCTGAAG; mouse GAPDH: forward, ATTGTCAGCAATGCATCCTG; reverse, ATGGACTGTGGTCATGAGCC; and human GAPDH: forward, AATGACCCCTTCATTGAC; reverse, TCCACGACGTACTCAGCGC. External standard curves were generated by dilution of the target PCR product purified by agarose gel electrophoresis. The absolute concentration of the external standard was measured with PicoGreen dsDNA Quantification Reagent (Molecular Probes, Eugene, OR).

Pharmacokinetic Analysis

Area under the curve (AUC) from 0 to 240 min after oral administration was calculated by trapezoidal method. Tissue-to-plasma or fetus-to-plasma concentration ratios (K_p values) were calculated by dividing tissue or fetus concentrations by plasma concentrations at 120-min postdose.

Immunohistochemical Analysis

Frozen sections of the testis and epididymis were prepared from FVB wild-type and *Bcrp*$^{-/-}$ mice and fixed to glass slides in methanol (−20°C). The sections were incubated in 1% Triton X-100 for 30 min at room temperature and subsequently washed with PBS three times. The sections were then incubated in PBS containing 5% bovine serum albumin (BSA-PBS) to block nonspecific protein binding. After washing with PBS three times, the sections were incubated with 1:40 dilution of anti-Bcrp monoclonal antibody (BXP-53; Signet Laboratories, Dedham, MA) in BSA-PBS at 4°C overnight. After washing with PBS three times, the sections were incubated with secondary antibody (Alexa 488 anti-rat IgG; Molecular Probes, Eugene, OR) and Topro3 (Molecular Probes) in BSA-PBS for 1 h at room temperature. The sections were mounted in VECTASHIELD mounting medium (Vector Laboratories, Burlingame, CA).

Statistical Analysis

Statistical analysis for significant differences was performed using the two-tailed Student's *t* test. A probability of <0.05 was considered to be statistically significant.

Results

In Vitro Transport of Phytoestrogens by mBcrp, hBCRP, and Mdr1a. The transport activities of daidzein, genistein, and coumestrol by mBcrp, hBCRP, and mMdr1a were investigated using transporter expressing cell systems (MDCK II/mBcrp, MDCK II/hBCRP, and L-Mdr1a). In those systems, mBcrp, hBCRP, and Mdr1a are localized in the apical membrane and direct the transcellular transport of their substrates in the apical direction (Smith et al., 1998; Matsushima et al., 2005). In MDCK II/mBcrp and MDCK II/hBCRP, the permeability of basal-to-apical direction was greater than that of apical-to-basal direction for all three phytoestrogens, whereas the transcellular transport was almost identical in both directions in MDCK II/GFP (Fig. 1 and Table 1). The flux ratios were higher in MDCK II/mBcrp and MDCK II/hBCRP than those in MDCK II/GFP, suggesting the three phytoestrogens are the substrate of mBcrp and hBCRP. In LLC-PK1 and L-Mdr1a, the permeability of basal-to-apical direction was slightly higher than that of apical-to-basal direction; however, the flux ratios were almost identical between the two cell systems, suggesting the three phytoestrogens are not the substrate of mMdr1a (Fig. 2 and Table 1).

Effects of Bcrp on the In Vivo Disposition of Phytoestrogens. Plasma levels of daidzein, genistein, and coumestrol after oral administration were compared between wild-type and *Bcrp*$^{-/-}$ mice (Fig. 3). Daidzein and genistein exhibited significantly higher plasma exposure in *Bcrp*$^{-/-}$ mice than in wild-type mice (Fig. 3A). The area under the curve over 4 h ($AUC_{0-240\ min}$) was 3.7- and 2.0-fold greater for daidzein and genistein, respectively, than the corresponding control values (Fig. 3B). The plasma exposure of coumestrol was very low compared with the other phytoestrogens, and no significant difference was observed in the $AUC_{0-240\ min}$ of coumestrol between the wild-type and *Bcrp*$^{-/-}$ mice, although significant changes were observed in plasma concentrations at several time points.

Tissue distributions of the phytoestrogens were determined at steady state achieved by a constant intravenous infusion (Fig. 4). Plasma concentrations were almost constant between 60 and 120 min, indicating that plasma concentrations reached a plateau at 60 min (Fig. 4A). The plasma concentrations of daidzein were significantly higher in *Bcrp*$^{-/-}$ mice than that in wild-type mice, but no significant changes were observed for genistein and coumestrol. The K_p values of brain and testis were significantly increased in *Bcrp*$^{-/-}$ mice for all of the three phytoestrogens (Fig. 4B). The fold increases in the K_p values of the brain were 5.6, 9.2, and 3.9 and those in the testis were 5.8, 5.8, and 4.1 for daidzein, genistein, and coumestrol, respectively. The K_p values of [^{14}C]inulin were investigated to estimate the volume of

the capillary space in the brain and testis. The K_p values of [^{14}C]inulin were 0.011 ± 0.004 and 0.031 ± 0.011 (mean ± S.E., n = 3) for the brain and testis, respectively (indicated by a broken line in Fig. 4B). In addition, the effects of Bcrp on the distributions of genistein in the epididymis and ovary were also investigated (Fig. 5). The K_p value of the epididy-

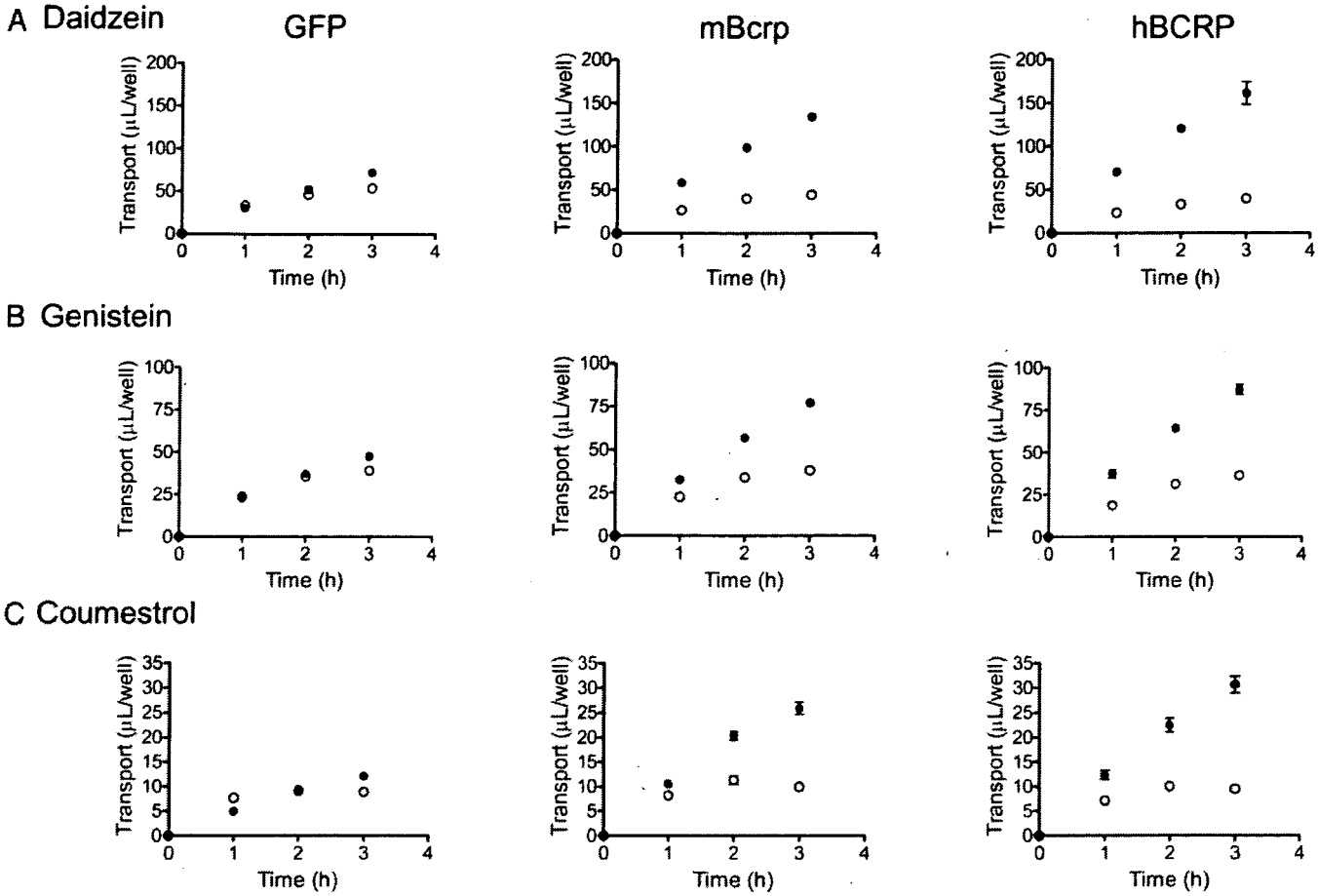

Fig. 1. The transcellular transport of daidzein (A), genistein (B), and coumestrol (C) across monolayers of MDCK II cells expressing the gene for GFP, mBcrp, and hBCRP. Transport in the apical-to-basal direction is represented by ○ and that in the basal-to-apical direction by ●. Data are represented by means ± S.E. of triplicate experiments.

TABLE 1

Transcellular transport of phytoestrogens across MDCK II monolayers expressing mBcrp and hBCRP and across LLC-PK1 monolayer expressing mMdr1a

Data are taken from Figs. 1 and 2. Each value represents the mean ± S.E. A to B represents the permeability of the transcellular transport in the apical to basal direction. B to A represents the permeability of the transcellular transport in the basal to apical direction.

Compound and Cell Line	Permeability		Flux Ratio
	A to B	B to A	
	μl/h/well		
Daidzein			
MDCKII/GFP	17.4 ± 0.2	23.7 ± 0.3	1.36
MDCKII/hBCRP	12.9 ± 0.7	53.2 ± 4.1	4.12
MDCKII/mBcrp	14.7 ± 0.3	44.1 ± 0.8	3.00
LLC-PK1	26.7 ± 1.2	49.9 ± 1.0	1.87
L-Mdr1a	27.9 ± 0.8	47.3 ± 1.0	1.70
Genistein			
MDCKII/GFP	13.0 ± 0.3	15.7 ± 0.4	1.21
MDCKII/hBCRP	12.2 ± 0.8	28.8 ± 1.0	2.36
MDCKII/mBcrp	12.5 ± 0.5	25.6 ± 0.3	2.05
LLC-PK1	54.0 ± 2.3	77.5 ± 0.8	1.44
L-Mdr1a	54.2 ± 1.1	76.0 ± 1.8	1.40
Coumestrol			
MDCKII/GFP	2.80 ± 0.04	4.08 ± 0.18	1.40
MDCKII/hBCRP	3.13 ± 0.15	10.2 ± 0.6	3.26
MDCKII/mBcrp	3.29 ± 0.23	8.75 ± 0.41	2.66
LLC-PK1	11.3 ± 0.4	18.7 ± 0.4	1.65
L-Mdr1a	18.9 ± 0.5	30.9 ± 0.6	1.63

mis was increased in *Bcrp*$^{-/-}$ mice with a fold increase of 2.5, whereas the K_p value of the ovary was unchanged.

Localization of Bcrp in Mouse Testis and Epididymis, and mRNA Expression of *BCRP* in the Human Epididymis. Immunohistochemical analysis was performed to identify the membrane localization of Bcrp protein in the testis and epididymis using the anti-Bcrp antibody (BXP-53) (Fig. 6). In the testis of wild-type mice, Bcrp was detected

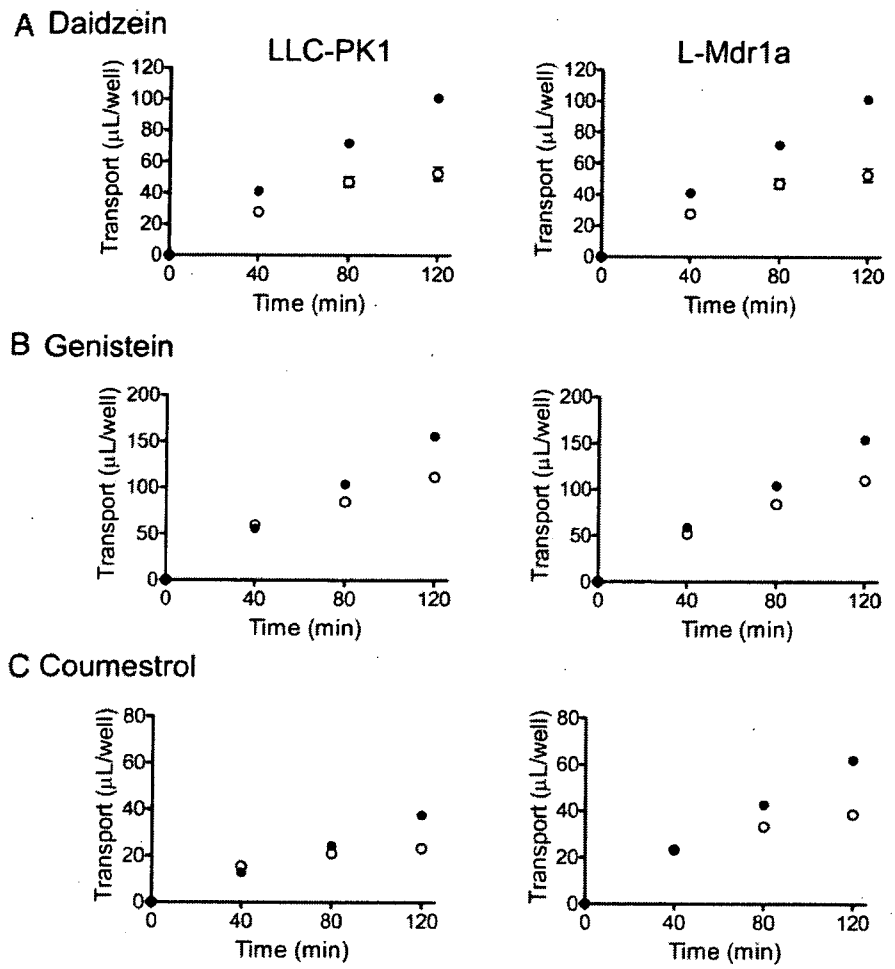

Fig. 2. The transcellular transport of daidzein (A), genistein (B), and coumestrol (C) across monolayers of control and mMdr1a-expressing LLC-PK1 cells. Transport in the apical-to-basal direction is represented by ○ and that in the basal-to-apical direction by ●. Data are represented by means ± S.E. of triplicate experiments.

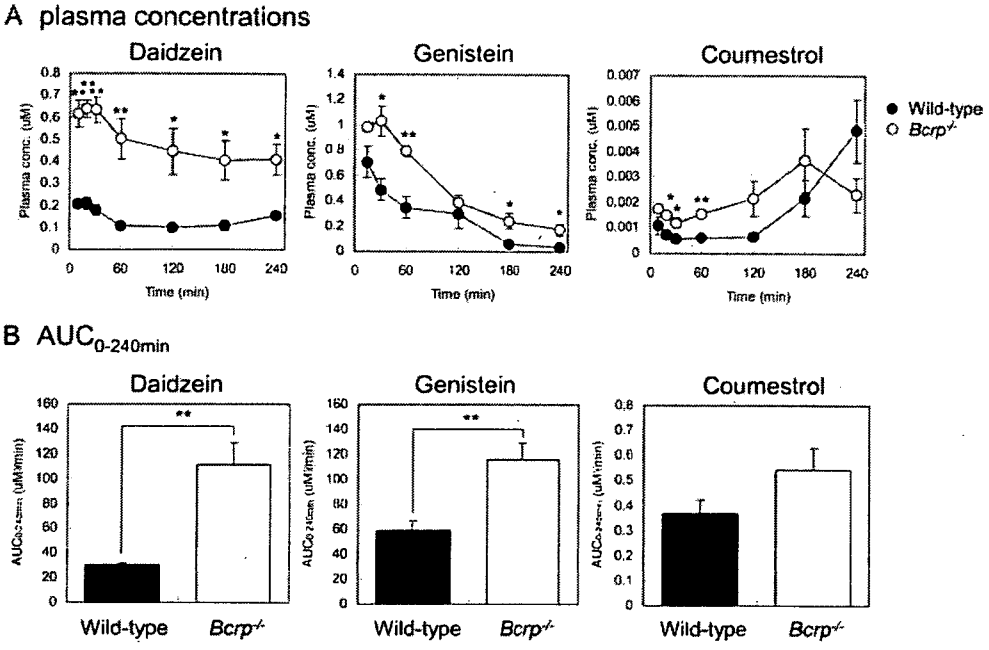

Fig. 3. Comparison of the plasma concentrations of daidzein, genistein, and coumestrol after oral administration (30 μmol/kg) of daidzein, genistein, or coumestrol between wild-type and *Bcrp*$^{-/-}$ mice. A, the time profiles of plasma concentrations. B, plasma AUC from time 0 to 240 min. Data are represented by means ± S.E. of three or four mice. Asterisks represent statistically significant differences between wild-type and *Bcrp*$^{-/-}$ mice: *, $P < 0.05$; **, $P < 0.01$.

only in the endothelial cells (Fig. 6A) and specifically in the luminal membrane (Fig. 6C). In the epididymis, the localization of Bcrp differed between the head and body regions (Fig. 6D). In the head (Fig. 6D, left), Bcrp was detected in both the luminal and abluminal sides of ducts, whereas in the body (Fig. 6D, right), Bcrp staining was observed in the endothelial cells. Immunofluorescence by BXP-53 was diminished in *Bcrp*$^{-/-}$ mice, indicating that the signals were associated specifically with Bcrp. We also examined the mRNA expression level of *BCRP* in the human epididymis. The ratio of *BCRP* mRNA to that of *GAPDH* was 1.16×10^{-2} and was similar to that found in the mouse epididymis (1.42×10^{-2}).

Role of Bcrp on the Accumulation of Genistein in the Fetus and Fetus Brain. Role of Bcrp on the fetal distribution of genistein was investigated in pregnant mice. Genistein was given to pregnant mice by constant intravenous infusion, and the plasma concentrations were similar between wild-type and *Bcrp*$^{-/-}$ mice (Fig. 7A). The fetus-to-maternal plasma concentration ratio was 1.8-fold greater in *Bcrp*$^{-/-}$ mice than controls (Fig. 7B). Brain-to-whole body concentration ratios were compared between wild-type and *Bcrp*$^{-/-}$ fetus to evaluate the Bcrp function in fetal blood-brain barrier. Brain-to-whole body concentration ratio was 1.4-fold increased in *Bcrp*$^{-/-}$ mice (Fig. 7C).

Discussion

In the present study, the role of Bcrp in limiting oral absorption of the phytoestrogens and their penetration into the brain, testis, epididymis, and fetus was investigated using *Bcrp*$^{-/-}$ mice. We tested three phytoestrogens, daidzein, genistein, and coumestrol. Daidzein and genistein are two major isoflavonoids in soy-based meal and are the most frequently ingested phytoestrogens. Coumestrol is known to be the most potent phytoestrogen. We found that all three phytoestrogens are substrates of Bcrp (Fig. 1). We also investigated the transport of the phytoestrogens by mMdr1a, which exhibits overlapped tissue distribution with Bcrp, and has been shown to limit the oral availability and tissue distributions of a variety of compounds. However, it was found that

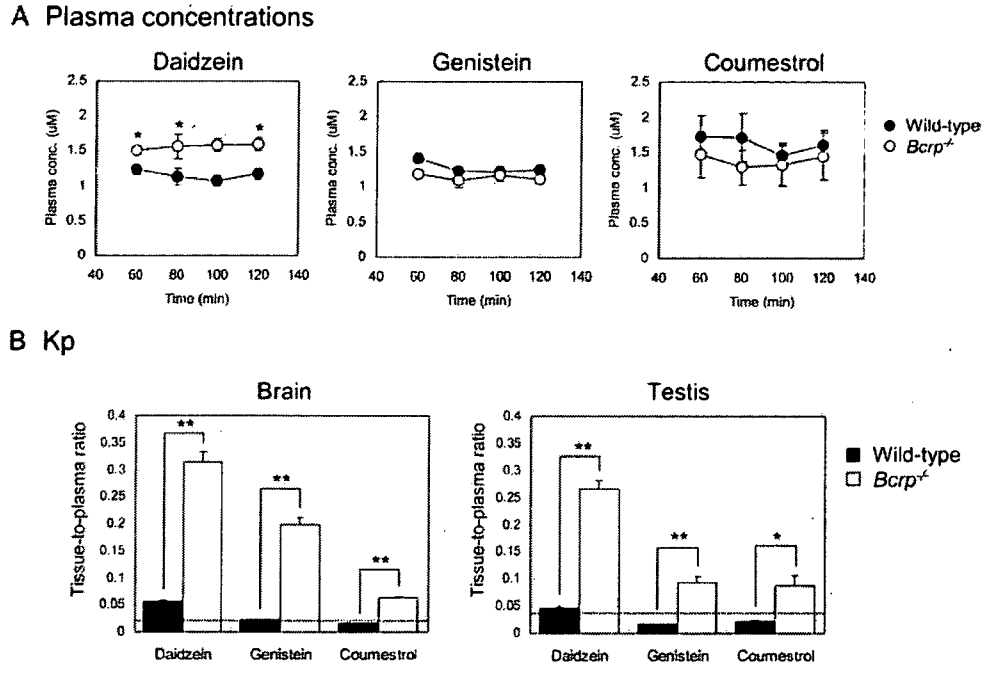

Fig. 4. Comparison of the brain and testis distributions of daidzein, genistein, or coumestrol between wild-type and *Bcrp*$^{-/-}$ mice. Compounds were infused intravenously at a dose rate of 5 μmol/h/kg, and K_p values in the brain and testis were measured at 120 min. A, the time profiles of plasma concentrations. B, K_p values in the brain and testis. K_p values of [^{14}C]inulin are represented by broken lines. Data are represented by means ± S.E. of three or four mice. Asterisks represent statistically significant differences between wild-type and *Bcrp*$^{-/-}$ mice; *, $P < 0.05$; **, $P < 0.01$.

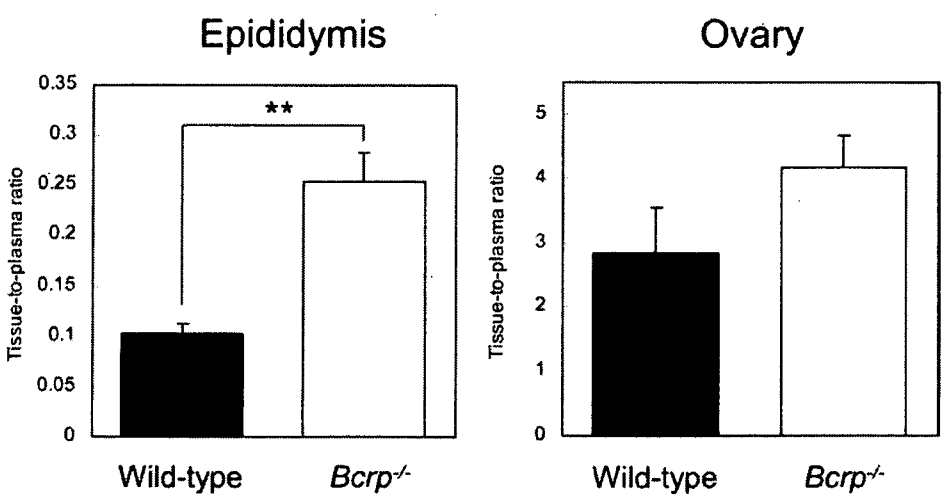

Fig. 5. Comparison of the epididymal and ovarian distributions of genistein between wild-type and *Bcrp*$^{-/-}$ mice. Genistein was infused intravenously at a dose rate of 5 μmol/h/kg, and K_p values in the epididymis and ovary were obtained at 120 min in male and female mice, respectively. Data are represented by means ± S.E. of three or four mice. Asterisks represent statistically significant differences between wild-type and *Bcrp*$^{-/-}$ mice: **, $P < 0.01$.

all three phytoestrogens were not the substrate of Mdr1a (Fig. 2).

After oral administration, the plasma AUC of daidzein and genistein was significantly increased in *Bcrp*$^{-/-}$ mice (Fig. 3, A and B). For coumestrol, the plasma concentrations exhibited a significant change in *Bcrp*$^{-/-}$ mice only at early time points, and thus, the AUC did not exhibit a statistically significant change. There are three potential sites to account for the increase in the plasma concentration after oral administration: an increase in intestinal absorption, and a decrease in intestinal and hepatic extraction. When given intravenously, the change in the plasma concentrations of phytoestrogens between wild-type and *Bcrp*$^{-/-}$ mice were marginal (Fig. 4). This is reasonable because the major elimination pathway of phytoestrogens from the systemic circulation is glucuronidation. Impaired Bcrp hardly affects the hepatic first-pass effect for phytoestrogens. Glucuronidation may be part of the mechanism limiting oral availability of the phytoestrogens as reported for quercetin (Crespy et al., 1999). We have reported that the intestinal glucuronidation activity of 4-methylumberifellone exhibited no change in *Bcrp*$^{-/-}$ mice (Enokizono et al., 2007). Therefore, the enhanced plasma exposure after oral administration in *Bcrp*$^{-/-}$ mice is probably due to an increased intestinal absorption. The effect of Bcrp on the oral availability of coumestrol was minimal, whereas the in vitro transport activity by mBcrp

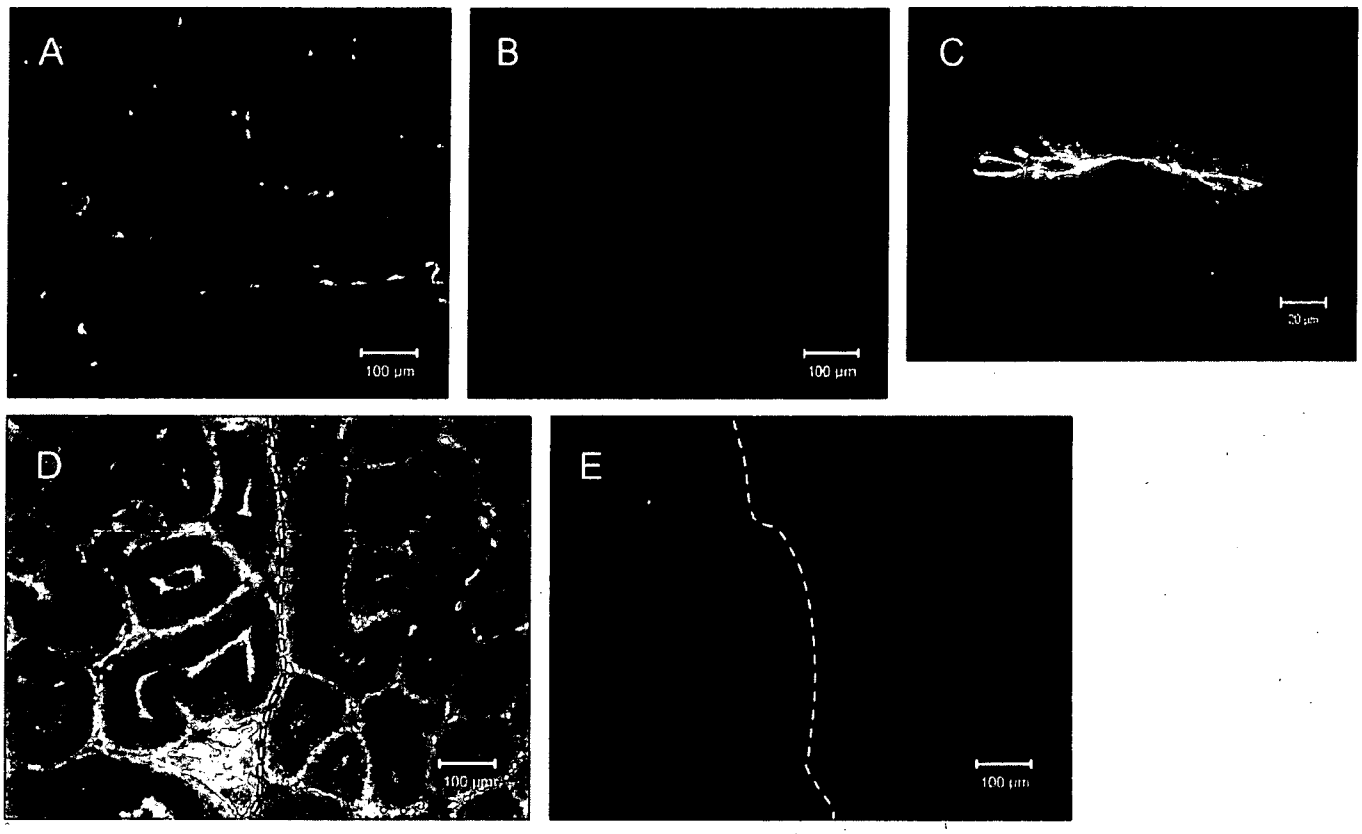

Fig. 6. Immunohistochemical analysis of Bcrp in the testis and epididymis. Localizations of Bcrp protein and DNA are shown by green and blue staining, respectively. A, testis of wild-type mice. B, testis of *Bcrp*$^{-/-}$ mouse. C, endothelial cells in the testis of wild-type mice. D, epididymis of wild-type mouse. E, epididymis of *Bcrp*$^{-/-}$ mouse. In D and E, the white lines discriminate the head (left) from the body (right).

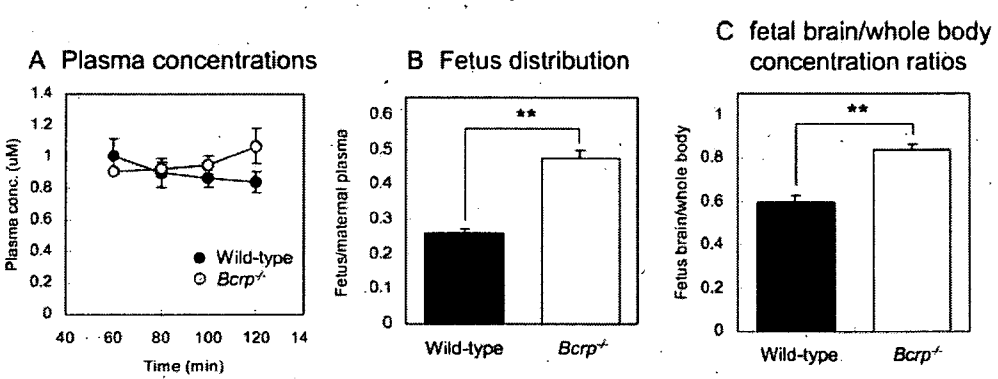

Fig. 7. Comparison of the distributions of genistein into the fetuses and fetal brain between wild-type and *Bcrp*$^{-/-}$ mice. Genistein was intravenously infused to pregnant mice at a dose rate of 5 μmol/h/kg, and the distributions into the fetuses and fetal brain were measured at 120 min. A, the time profiles of plasma concentrations. B, fetus-to-maternal plasma concentration ratios. C, brain-to-whole body concentration ratios in fetal mice. Data are represented by means ± S.E. of three mice. Asterisks represent statistically significant differences between wild-type and *Bcrp*$^{-/-}$ mice: **, $P < 0.01$.

was similar among the three phytoestrogens (Fig. 1). This indicates the smaller contribution of Bcrp to the intestinal absorption of coumestrol. The contribution of paracellular transport and intestinal metabolism may be greater for coumestrol than the other phytoestrogens. Indeed, transcellular transport of coumestrol in the apical-to-basal direction in control cells (MDCKII/GFP and LLC-PK1) was lowest among the three phytoestrogens, suggesting the lowest transcellular transport of coumestrol. The mechanism governing the increased plasma concentrations of daidzein during intravenous infusion in *Bcrp*$^{-/-}$ mice remains unknown. Impaired urinary excretion could be one possible mechanism because daidzein also undergoes urinary excretion: approximately 10% of the dose after oral administration (Bayer et al., 2001).

The K_p values of brain and testis of all three phytoestrogens were significantly increased in *Bcrp*$^{-/-}$ mice (Fig. 4B). Considering that the K_p values of the phytoestrogens and [^{14}C]inulin were similar in wild-type mice, the brain and testis distribution of the phytoestrogens is almost completely limited by Bcrp. Bcrp has been identified on the luminal membrane of both the human and mouse brain capillary endothelial cells that form the blood-brain barrier (Cooray et al., 2002; Lee et al., 2005), whereas there is an interspecies difference in membrane localization in the testis. Bcrp is localized on both the luminal side of the endothelial cells and the apical membrane of myoid cells in the human testis (Bart et al., 2004), whereas Bcrp expression is restricted to the luminal membrane of capillary-like structures in the mouse testis (Fig. 6, A and C). It is generally considered that the Sertoli and myoid cells form the blood-testis barrier, but endothelial cell-cell junctions are more leaky in rats (Dym and Fawcett, 1970). However, from the present results, testicular endothelial cells evidently have an adequate barrier function against phytoestrogens, at least in mice.

In addition to the testis, we investigated the role of Bcrp in other reproductive organs, the epididymis and ovary. The epididymis is divided into three segments (head, body, and tail). Sperm formed in the testis enter the head and finally reach the tail. During this transition, they undergo maturation and are finally stored in the tail region. It was found that the distribution of genistein was also increased in the epididymis of *Bcrp*$^{-/-}$ mice (Fig. 5). Therefore, we propose that Bcrp limits the penetration of genistein into the epididymis. The membrane localization of Bcrp was regionally dependent in the epididymis. Bcrp was mainly localized in capillary-like structures in the body (Fig. 6D, left), whereas Bcrp was found both in the luminal and abluminal membranes of the ducts in the head (Fig. 6D, right). Bcrp in the capillary-like structure and the abluminal membranes of ducts may contribute to the reduced distribution of genistein in wild-type mice. The physiological role of the Bcrp in the luminal membranes of the ducts in the head is unknown. It may mediate the luminal secretion of some endogenous compounds. Unlike male reproductive organs, the ovaries did not exhibit any change in the tissue distribution of genistein (Fig. 5), although the *Bcrp* mRNA level in the ovaries is similar to that in the testis (Tanaka et al., 2005). The reason for the discrepancy between mRNA expression and functional activity in the ovaries remains unknown.

Fetal and newborn mice are more sensitive to estrogen than adults. The distribution of genistein in the fetus was increased in pregnant *Bcrp*$^{-/-}$ mice (Fig. 7B), suggesting that Bcrp limits the penetration of genistein into the fetus in the placenta. Furthermore, the brain-to-whole body concentration ratio was also increased in fetal *Bcrp*$^{-/-}$ mice (Fig. 7C). Therefore, fetal brain capillaries may develop a barrier function to some degree even at this stage. The smaller increase (1.4-fold) than that observed in adult mice (9.2-fold) suggests that the barrier function is still immature at this stage (Nico et al., 1999). Taken together, the exposure of phytoestrogens to the fetal brain is limited by Bcrp in the fetal blood-brain barrier, the placenta, and the maternal small intestine.

Estrogen plays a key role in the development of reproductive systems, and sexual differentiation and estrogenic chemicals are known to influence reproductive functions, such as reduced testicular weight, sperm counts, induction of the acrosome reaction in both human and mouse (Atanassova et al., 2000; Adeoya-Osiguwa et al., 2003; Kyselova et al., 2004; Fraser et al., 2006), and adult sexual behavior, such as reduced mounting and ejaculation in males and reduced lordosis in females (Patisaul et al., 2004). Bcrp will prevent these adverse effects of phytoestrogens by limiting the exposure to the reproductive organs and brain.

In conclusion, we have demonstrated the importance of Bcrp in limiting the oral availability of phytoestrogens and their penetration into the brain and male reproductive organs. In addition, Bcrp also limited the exposure of the mouse fetus to phytoestrogens by extruding them to the blood from the placenta. These results indicate the important roles of Bcrp in protecting the body from the adverse effects of phytoestrogens on sexual behavior and spermatogenesis.

Acknowledgments

We thank Dr. Alfred H. Schinkel (The Netherlands Cancer Institute, The Netherlands) for supplying *Bcrp*$^{-/-}$ mice and L-Mdr1a cells.

References

Adeoya-Osiguwa SA, Markoulaki S, Pocock V, Milligan SR, and Fraser LR (2003) 17beta-Estradiol and environmental estrogens significantly affect mammalian sperm function. *Hum Reprod* **18**:100–107.

Adlercreutz H (1995) Phytoestrogens: epidemiology and a possible role in cancer protection. *Environ Health Perspect* **103 Suppl 7**:103–112.

Atanassova N, McKinnell C, Turner KJ, Walker M, Fisher JS, Morley M, Millar MR, Groome NP, and Sharpe RM (2000) Comparative effects of neonatal exposure of male rats to potent and weak (environmental) estrogens on spermatogenesis at puberty and the relationship to adult testis size and fertility: evidence for stimulatory effects of low estrogen levels. *Endocrinology* **141**:3898–3907.

Bart J, Hollema H, Groen HJ, de Vries EG, Hendrikse NH, Sleijfer DT, Wegman TD, Vaalburg W, and van der Graaf WT (2004) The distribution of drug-efflux pumps, P-gp, BCRP, MRP1 and MRP2, in the normal blood-testis barrier and in primary testicular tumours. *Eur J Cancer* **40**:2064–2070.

Bayer T, Colnot T, and Dekant W (2001) Disposition and biotransformation of the estrogenic isoflavone daidzein in rats. *Toxicol Sci* **62**:205–211.

Breedveld P, Pluim D, Cipriani G, Wielinga P, van Tellingen O, Schinkel AH, and Schellens JH (2005) The effect of Bcrp1 (Abcg2) on the in vivo pharmacokinetics and brain penetration of imatinib mesylate (Gleevec): implications for the use of breast cancer resistance protein and P-glycoprotein inhibitors to enable the brain penetration of imatinib in patients. *Cancer Res* **65**:2577–2582.

Breedveld P, Zelcer N, Pluim D, Sonmezer O, Tibben MM, Beijnen JH, Schinkel AH, van Tellingen O, Borst P, and Schellens JH (2004) Mechanism of the pharmacokinetic interaction between methotrexate and benzimidazoles: potential role for breast cancer resistance protein in clinical drug-drug interactions. *Cancer Res* **64**:5804–5811.

Cassidy A, Bingham S, and Setchell K (1995) Biological effects of isoflavones in young women: importance of the chemical composition of soybean products. *Br J Nutr* **74**:587–601.

Chang HC, Churchwell MI, Delclos KB, Newbold RR, and Doerge DR (2000) Mass spectrometric determination of Genistein tissue distribution in diet-exposed Sprague-Dawley rats. *J Nutr* **130**:1963–1970.

Chen J, Wang S, Jia X, Bajimaya S, Lin H, Tam VH, and Hu M (2005) Disposition of flavonoids via recycling: comparison of intestinal versus hepatic disposition. *Drug Metab Dispos* **33**:1777–1784.

Cooray HC, Blackmore CG, Maskell L, and Barrand MA (2002) Localisation of breast cancer resistance protein in microvessel endothelium of human brain. *Neuroreport* **13**:2059–2063.

Crespy V, Morand C, Manach C, Besson C, Demigne C, and Remesy C (1999) Part of quercetin absorbed in the small intestine is conjugated and further secreted in the intestinal lumen. *Am J Physiol* **277**:G120–G126.

Delclos KB, Bucci TJ, Lomax LG, Latendresse JR, Warbritton A, Weis CC, and Newbold RR (2001) Effects of dietary genistein exposure during development on male and female CD (Sprague-Dawley) rats. *Reprod Toxicol* **15**:647–663.

Doerge DR, Churchwell MI, Chang HC, Newbold RR, and Delclos KB (2001) Placental transfer of the soy isoflavone genistein following dietary and gavage administration to Sprague-Dawley rats. *Reprod Toxicol* **15**:105–110.

Dym M and Fawcett DW (1970) The blood-testis barrier in the rat and the physiological compartmentation of the seminiferous epithelium. *Biol Reprod* **3**:308–326.

Enokizono J, Kusuhara H, and Sugiyama Y (2007) Regional expression and activity of breast cancer resistance protein (ABCG2) in mouse intestine: overlapped distribution with sulfotransferases. *Drug Metab Dispos* **35**:922–928.

Fraser LR, Beyret E, Milligan SR, and Adeoya-Osiguwa SA (2006) Effects of estrogenic xenobiotics on human and mouse spermatozoa. *Hum Reprod* **21**:1184–1193.

Hirano M, Maeda K, Matsushima S, Nozaki Y, Kusuhara H, and Sugiyama Y (2005) Involvement of BCRP (ABCG2) in the biliary excretion of pitavastatin. *Mol Pharmacol* **68**:800–807.

Imai Y, Tsukahara S, Asada S, and Sugimoto Y (2004) Phytoestrogens/flavonoids reverse breast cancer resistance protein/ABCG2-mediated multidrug resistance. *Cancer Res* **64**:4346–4352.

Jonker JW, Buitelaar M, Wagenaar E, Van Der Valk MA, Scheffer GL, Scheper RJ, Plosch T, Kuipers F, Elferink RP, Rosing H, et al. (2002) The breast cancer resistance protein protects against a major chlorophyll-derived dietary phytotoxin and protoporphyria. *Proc Natl Acad Sci U S A* **99**:15649–15654.

Kondo C, Suzuki H, Itoda M, Ozawa S, Sawada J, Kobayashi D, Ieiri I, Mine K, Ohtsubo K, and Sugiyama Y (2004) Functional analysis of SNPs variants of BCRP/ABCG2. *Pharm Res* **21**:1895–1903.

Kyselova V, Peknicova J, Boubelik M, and Buckiova D (2004) Body and organ weight, sperm acrosomal status and reproduction after genistein and diethylstilbestrol treatment of CD1 mice in a multigenerational study. *Theriogenology* **61**:1307–1325.

Lee YJ, Kusuhara H, Jonker JW, Schinkel AH, and Sugiyama Y (2005) Investigation of efflux transport of dehydroepiandrosterone sulfate and mitoxantrone at the mouse blood-brain barrier: a minor role of breast cancer resistance protein. *J Pharmacol Exp Ther* **312**:44–52.

Maliepaard M, Scheffer GL, Faneyte IF, van Gastelen MA, Pijnenborg AC, Schinkel AH, van De Vijver MJ, Scheper RJ, and Schellens JH (2001) Subcellular localization and distribution of the breast cancer resistance protein transporter in normal human tissues. *Cancer Res* **61**:3458–3464.

Matsushima S, Maeda K, Kondo C, Hirano M, Sasaki M, Suzuki H, and Sugiyama Y (2005) Identification of the Hepatic efflux transporters of organic anions using double-transfected Madin-Darby canine kidney II cells expressing human organic anion-transporting polypeptide 1B1 (OATP1B1)/multidrug resistance-associated protein 2, OATP1B1/multidrug resistance 1, and OATP1B1/breast cancer resistance protein. *J Pharmacol Exp Ther* **314**:1059–1067.

Mizuno N, Suzuki M, Kusuhara H, Suzuki H, Takeuchi K, Niwa T, Jonker JW, and Sugiyama Y (2004) Impaired renal excretion of 6-hydroxy-5,7-dimethyl-2-methylamino-4-(3-pyridylmethyl) benzothiazole (E3040) sulfate in breast cancer resistance protein (BCRP1/ABCG2) knockout mice. *Drug Metab Dispos* **32**:898–901.

Mueller SO, Simon S, Chae K, Metzler M, and Korach KS (2004) Phytoestrogens and their human metabolites show distinct agonistic and antagonistic properties on estrogen receptor alpha (ERalpha) and ERbeta in human cells. *Toxicol Sci* **80**:14–25.

Nico B, Quondamatteo F, Herken R, Marzullo A, Corsi P, Bertossi M, Russo G, Ribatti D, and Roncali L (1999) Developmental expression of ZO-1 antigen in the mouse blood-brain barrier. *Brain Res Dev Brain Res* **114**:161–169.

Patisaul HB, Luskin JR, and Wilson ME (2004) A soy supplement and tamoxifen inhibit sexual behavior in female rats. *Horm Behav* **45**:270–277.

Setchell KD, Brown NM, Zimmer-Nechemias L, Brashear WT, Wolfe BE, Kirschner AS, and Heubi JE (2002) Evidence for lack of absorption of soy isoflavone glycosides in humans, supporting the crucial role of intestinal metabolism for bioavailability. *Am J Clin Nutr* **76**:447–453.

Sfakianos J, Coward L, Kirk M, and Barnes S (1997) Intestinal uptake and biliary excretion of the isoflavone genistein in rats. *J Nutr* **127**:1260–1268.

Smith AJ, Mayer U, Schinkel AH, and Borst P (1998) Availability of PSC833, a substrate and inhibitor of P-glycoproteins, in various concentrations of serum. *J Natl Cancer Inst* **90**:1161–1166.

Tanaka Y, Slitt AL, Leazer TM, Maher JM, and Klaassen CD (2005) Tissue distribution and hormonal regulation of the breast cancer resistance protein (Bcrp/Abcg2) in rats and mice. *Biochem Biophys Res Commun* **326**:181–187.

van Herwaarden AE, Jonker JW, Wagenaar E, Brinkhuis RF, Schellens JH, Beijnen JH, and Schinkel AH (2003) The breast cancer resistance protein (Bcrp1/Abcg2) restricts exposure to the dietary carcinogen 2-amino-1-methyl-6-phenylimidazo[4,5-b]pyridine. *Cancer Res* **63**:6447–6452.

Watanabe S, Terashima K, Sato Y, Arai S, and Eboshida A (2000) Effects of isoflavone supplement on healthy women. *Biofactors* **12**:233–241.

Whitten PL, Patisaul HB, and Young LJ (2002) Neurobehavioral actions of coumestrol and related isoflavonoids in rodents. *Neurotoxicol Teratol* **24**:47–54.

Wisniewski AB, Klein SL, Lakshmanan Y, and Gearhart JP (2003) Exposure to genistein during gestation and lactation demasculinizes the reproductive system in rats. *J Urol* **169**:1582–1586.

Zhang W, Mojsilovic-Petrovic J, Andrade MF, Zhang H, Ball M, and Stanimirovic DB (2003) The expression and functional characterization of ABCG2 in brain endothelial cells and vessels. *FASEB J* **17**:2085–2087.

Address correspondence to: Dr. Yuichi Sugiyama, Graduate School of Pharmaceutical Sciences, The University of Tokyo, 7-3-1, Hongo, Bunkyo-ku, Tokyo 113-0033, Japan. E-mail: sugiyama@mol.f.u-tokyo.ac.jp

0026-895X/07/7206-1619–1625
MOLECULAR PHARMACOLOGY
U.S. Government work not protected by U.S. copyright
Mol Pharmacol 72:1619–1625, 2007

Vol. 72, No. 6
39701/3277936
Printed in U.S.A.

Regulation of Tissue-Specific Expression of the Human and Mouse Urate Transporter 1 Gene by Hepatocyte Nuclear Factor 1 α/β and DNA Methylation

Ryota Kikuchi, Hiroyuki Kusuhara, Naka Hattori, Insook Kim, Kunio Shiota, Frank J. Gonzalez, and Yuichi Sugiyama

Department of Molecular Pharmacokinetics, Graduate School of Pharmaceutical Sciences, the University of Tokyo, Tokyo, Japan (R.K., H.K., Y.S.); Laboratory of Cellular Biochemistry, Department of Animal Resource Sciences/Veterinary Medical Sciences, the University of Tokyo, Tokyo, Japan (N.H., K.S.); Laboratory of Metabolism, National Cancer Institute, National Institutes of Health, Bethesda, Maryland (I.K., F.J.G.)

Received July 6, 2007; accepted September 10, 2007

ABSTRACT

Expression of Urate transporter 1 (URAT1/*SLC22A12*) is restricted to the proximal tubules in the kidney, where it is responsible for the tubular reabsorption of urate. To elucidate the mechanism underlying its tissue-specific expression, the transcriptional regulation of the *hURAT1* and *mUrat1* genes was investigated. Hepatocyte nuclear factor 1 α (HNF1α) and HNF1β positively regulate minimal promoter activity of the *URAT1* gene as shown by reporter gene assays. Electrophoretic mobility shift assays revealed binding of HNF1α and/or HNF1β to the HNF1 motif in the *hURAT1* promoter. Furthermore, the mRNA expression of Urat1 is reduced in the kidneys of *Hnf1*α-null mice compared with wild-type mice, confirming the indispensable role of HNF1α in the constitutive expression of *URAT1* genes. It was also shown that the proximal promoter region of *mUrat1* was hypermethylated in the liver and kidney medulla, whereas this region was relatively hypomethylated in the kidney cortex. These methylation profiles are in a good agreement with the proximal tubule-restricted expression of mUrat1 in the kidney cortex. Taken together, these results strongly suggest that tissue-specific expression of the *URAT1* genes is coordinately regulated by the transcriptional activation by HNF1α/HNF1β heterodimer and repression by DNA methylation.

Urate is an end product of purine metabolism in humans and other higher primates. It is generally recognized that urate works as a scavenger of potentially harmful radicals in the human body. However, hyperuricemia can be associated with health problems such as gout, nephrolithiasis, hypertension, and vascular disease, whereas hypouricemia is primarily characterized by exercise-induced acute renal failure. Thus, the serum urate level must be tightly regulated through complex renal handling processes, which is historically explained by a four-component model (i.e., glomerular filtration, tubular secretion, and pre- and postsecretory reabsorption). After these processes, approximately 90% of the urate filtered through the glomerulus is reabsorbed in humans (Rafey et al., 2003; Enomoto and Endou, 2005; Hediger et al., 2005).

Urate transporter 1 (URAT1/*SLC22A12*) is a membrane transporter responsible for the reabsorption of urate in the apical membrane of the renal proximal tubules (Enomoto et al., 2002). Mutations in the *URAT1* gene, causing functional impairment, are associated with idiopathic renal hypouricemia (Enomoto et al., 2002; Iwai et al., 2004). In addition, fractional excretion of urate in patients with homozygous or compound heterozygous *SLC22A12* mutations is not sensitive to uricosuric (probenecid and benzbromarone) and antiuricosuric (pyrazinamide) drugs, suggesting that these drugs target URAT1 to exert their effects in vivo (Ichida et al., 2004). The mouse homolog of hURAT1, mUrat1, shows the same tissue distribution as that of hURAT1 and is probably involved in the reabsorption of urate in the kidney (Hosoyamada et al., 2004). It can also be an exit pathway for

Article, publication date, and citation information can be found at http://molpharm.aspetjournals.org.
doi:10.1124/mol.107.039701.

ABBREVIATIONS: OAT, organic anion transporter; URAT1, urate transporter 1; HNF1, hepatocyte nuclear factor 1; PCR, polymerase chain reaction; Gapdh, glyceraldehyde-3-phosphate dehydrogenase; T-DMR, tissue-dependent differentially methylated region; MODY, maturity-onset diabetes of the young; HEK, human embryonic kidney; wt, wild-type hepatocyte nuclear factor 1 motif in the *hURAT1* promoter; per, the consensus sequence for the hepatocyte nuclear factor 1 motif; mut, mutated hepatocyte nuclear factor 1 motif; m, mouse; h, human.

several anionic drugs in the proximal tubules together with the basolateral uptake transporters [organic anion transporter (Oat) 1 and Oat3] (Imaoka et al., 2004).

A previous report suggested the presence of a hepatocyte nuclear factor 1 (HNF1) binding motif in the minimal promoter region of the *hURAT1* gene, which is conserved in the proximal promoters of rodent *Urat1* genes (Li et al., 2004). HNF1 is known to regulate transcription of many hepatic genes by forming homodimers or heterodimers between two isoforms, HNF1α and HNF1β (Mendel and Crabtree, 1991; Tronche and Yaniv, 1992). Their expression in the kidney and a renal Fanconi syndrome or polycystic kidney disease in *Hnf1*α- or kidney-specific *Hnf1*β-null mice, respectively, also imply a role for these transcription factors in the kidney (Pontoglio et al., 1996; Gresh et al., 2004). We have found recently that HNF1α/β is a potent transactivator of the human and mouse *OAT3* promoter (Kikuchi et al., 2006). Then it was reported that the mRNA levels of several drug transporters, including Oat1 and Oat3, are reduced in the kidney of *Hnf1*α-null mice, further confirming the involvement of HNF1α in the transcriptional regulation of drug transporters in the kidney (Maher et al., 2006). The functional importance of HNF1 in the regulation of the *URAT1* gene has yet to be investigated. However, considering that the serum levels of urate are reduced and the renal fractional excretion is increased in *Hnf1*α-null mice (Pontoglio et al., 1996), it is possible that HNF1α directly regulates URAT1 expression.

HNF1α and HNF1β are expressed in the polarized epithelia of a variety of tissues, including liver, kidney, intestine, stomach, and pancreas (Blumenfeld et al., 1991; De Simone et al., 1991). Thus, positive regulation by HNF1 alone cannot account for the predominant expression of URAT1 in the kidney. Our previous study suggests that the expression of hOAT3 is negatively regulated by DNA methylation in addition to the positive regulation by HNF1α and HNF1β (Kikuchi et al., 2006). DNA methylation is one of the most well-characterized mechanisms underlying the epigenetic regulation of gene expression (Bird, 2002; Shiota, 2004). Methylation of the cytosine residue in the CpG dinucleotide negatively regulates gene transcription through the recruitment of chromatin remodeling factors, and many reports highlight the key role of DNA methylation in tissue-specific gene transcription. Because several CpG dinucleotides were found in the 5′-flanking region of *hURAT1* and *mUrat1* (Fig. 1), it is of great interest to determine whether the concerted effect of DNA methylation and HNF1α/β regulates tissue-specific expression of these genes. The present study was aimed to clarify the involvement of HNF1α and HNF1β as genetic factors and DNA methylation as an epigenetic factor in the tissue-specific expression of human and mouse *URAT1* genes.

Materials and Methods

Isolation of the 5′-Flanking Sequence of *hURAT1* and *mUrat1* Gene. The minimal promoter region of *hURAT1* gene (−253/+83) (Li et al., 2004) was amplified by PCR using human genomic DNA as a template and the forward (h − 253) and reverse (h + 83) primers with an artificial KpnI and HindIII site, respectively (Table 1). The PCR product was subcloned into the KpnI and HindIII restriction sites of pGL3-Basic (Promega, Madison, WI), yielding the *hURAT1* minimal promoter construct, hURAT1_−253/+83-HNF1wt. The transcriptional start site of the *mUrat1* gene was determined using the public database Database of Transcriptional Start Sites (available at http://dbtss.hgc.jp/) with the ref sequence identification for mUrat1 (NM_009203), and based on high homology with the 5′-flanking region of *hURAT1* (Fig. 1). Because the position of transcriptional start site in the clone MS2926204 is nearest to that of *hURAT1* transcriptional start site, which was experimentally determined in the previous report, we chose this site as the transcriptional start site of *mUrat1* gene. The *mUrat1* putative promoter region was isolated from mouse genomic

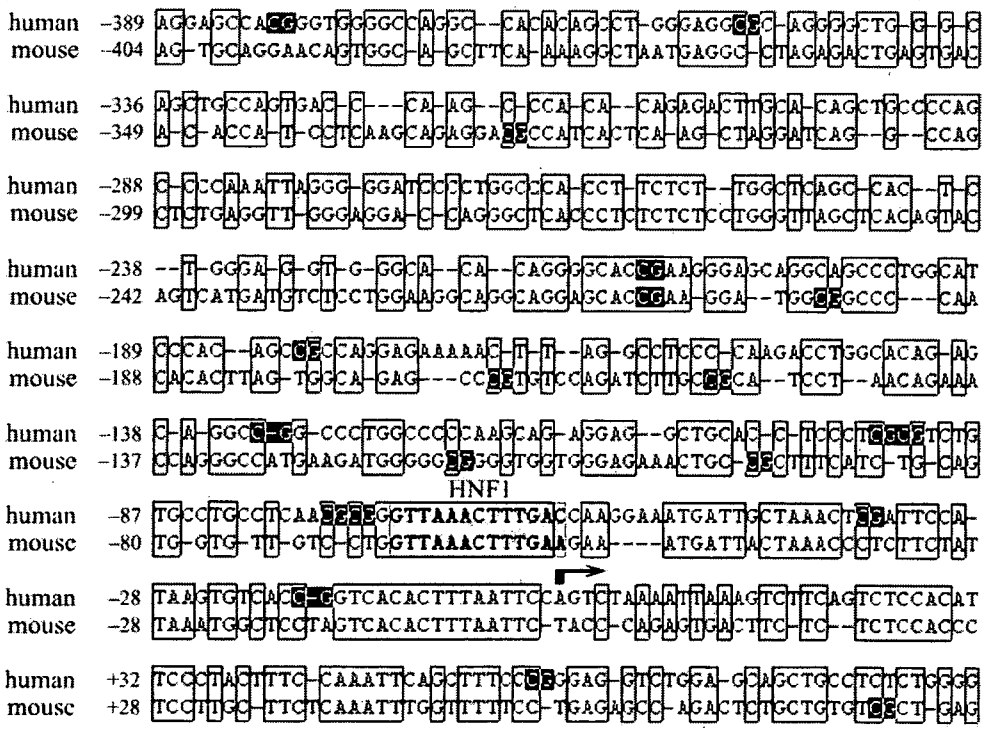

Fig. 1. Alignment of the proximal promoter of human and mouse *URAT1*. Nucleotide sequences of the proximal promoter region of human and mouse *URAT1* genes were aligned using Genetyx version 8 to show the high homology of the 5′-flanking region between species. Nucleotide numberings are relative to the transcriptional start sites indicated by an arrow (+1), and homologous sequences between species are boxed. Canonical HNF1 binding motif in the promoter is shaded, and CpG dinucleotides in each sequence are reverse-colored.

DNA by a PCR-based approach using the forward (m − 261) and reverse (m + 80) primers (Table 1). The PCR product was subcloned into pGL3-Basic as described above, yielding mUrat1_−260/+80. The sequences of all constructs were verified by DNA sequencing.

Site-Directed Mutagenesis. Mutations in the HNF1 motif located within the *hURAT1* minimal promoter were introduced using the QuikChange XL Site-Directed Mutagenesis Kit (Stratagene, La Jolla, CA) with internal mutated oligonucleotides (Table 1). The introduction of mutations was verified by DNA sequencing.

RNA Isolation and Quantitative PCR. Total RNA was isolated from the kidneys of 7- to 14-week-old male (n = 3) and female (n = 4) wild-type or *Hnf1α*-null adult mice (Lee et al., 1998) and treated with DNase I to remove the contaminated genomic DNA, followed by reverse-transcription using a random-nonamer primer (Takara, Shiga, Japan). To quantify the mRNA expression of mUrat1 in wild-type or *Hnf1α*-null mice, real-time quantitative PCR was performed as described previously using the primers shown in Table 1 (Kikuchi et al., 2006). The mRNA expression of mUrat1 was normalized by the mRNA expression of Gapdh and statistically analyzed by Student's t test. Asterisks (* and **) represent significant differences ($P < 0.05$ and $P < 0.01$, respectively) between wild-type and *Hnf1α*-null mice of each gender.

Cell Culture and Transfections. Cell culture, transfections, and luciferase assays were performed as described previously (Kikuchi et al., 2006). For transactivation assays in HEK293 cells, 5 ng of empty pcDNA3.1(+) vector, 5 ng of HNF1α expression vector, 2.5 ng of HNF1α and HNF1β expression vectors, or 5 ng of HNF1β expression vector was cotransfected with 0.5 μg of the corresponding promoter construct and 0.05 μg of internal standard pRL-SV40. The promoter activity was measured as relative light units of firefly luciferase per unit of *Renilla reniformis* luciferase.

Preparation of Nuclear Extracts and Electrophoretic Mobility Shift Assay. Nuclear extracts were prepared from HepG2, Caco-2, and HEK293 parent cells, or HEK293 cells transiently transfected with pcDNA3.1(+), either HNF1α or HNF1β expression vector, or both expression vectors as described previously (Kikuchi et al., 2006). Transient transfection of the expression vectors into HEK293 cells was performed using FuGENE6 (Roche Diagnostics, Indianapolis, IN) according to the manufacturer's instructions. Three kinds of double-stranded oligonucleotides (wt, per, and mut) were obtained by hybridizing the single-stranded complementary oligonucleotide with sense sequences shown in Table 1. Sequence "wt" corresponds to the wild-type HNF1 motif in the *hURAT1* promoter, and "per" corresponds to the perfect consensus sequence for the HNF1 motif, whereas "mut" denotes the wild-type sequence mutated within the motif. Five micrograms of nuclear extracts from HepG2, Caco-2, or HEK293 parent cells or 3 μg of nuclear extracts form HEK293 cells transfected with several expression vectors was used in the electrophoretic mobility shift assays. Competition and supershift assays were performed as described previously with Dig Gel Shift Kit, Second Generation (Roche Diagnostics).

Sodium Bisulfite Genomic Sequencing. Genomic DNA from liver, kidney cortex, or kidney medulla of ddY male mice at 8 weeks of age was extracted using a Get Pure DNA Kit (Dojindo Molecular Technologies, Gaithersburg, MD). One microgram of genomic DNA digested with EcoRI was denatured by adding NaOH to give a final concentration of 0.3 M and was incubated for 15 min at 37°C. After the incubation, sodium metabisulfite, pH 5.0, and hydroquinone were added to give final concentrations of 2.0 M and 0.5 mM, respectively, and the mixture was incubated for 16 h at 55°C in the dark. The modified DNA was purified using the Wizard DNA Clean-Up System (Promega), and the bisulfite reaction was terminated by adding NaOH to give a final concentration of 0.3 M and incubating for 15 min at 37°C. The solution was neutralized by adding NH_4OAc, pH 7.0, and the DNA was ethanol-precipitated, dried, and resuspended in 10 mM Tris-HCl and 1 mM EDTA, pH 8.0. The DNA fragment covering the proximal promoter region of the *mUrat1* gene was amplified by PCR using the following primers: −419-B-F, and +134-B-R (Table 1). The PCR products were cloned into pGEM-T Easy vector (Promega), and 10 clones randomly picked from each of two independent PCRs were sequenced to determine the presence of methylated cytosines.

TABLE 1

Oligonucleotides used for the production of promoter fragments, mobility shift assays, site-directed mutagenesis, quantitative PCR, and bisulfite PCR

Regarding the oligonucleotides used for the mobility shift assays and site-directed mutagenesis, the HNF1-motif in the *hURAT1* promoter region is underlined. Boldface type indicates the difference in the sequence of the per and mut compared with the wild-type sequence found in the *hURAT1* promoter.

Oligonucleotide	Orientation	Sequence (5′ to 3′)
Primers used for the cloning of 5′-flanking regions		
hURAT1		
h − 253	Forward	CGGGGTACCTTGGCTCAGCCACTCTGGGAGGT
h + 83	Reverse	CCCAAGCTTAGAGAGGCAGCTGCTCCAGACC
mUrat1		
m − 261	Forward	CGGGGTACCCTGGGTTAGCTCACAGTACAG
m + 80	Reverse	CCCAAGCTTAGCGACACAGCAGAGTCTG
Oligonucleotides used for the construction of EMSA probe and competitor or site-directed mutagenesis		
wt	Sense	CTCAACGCGGGTTAAACTTTGACCAAGGAAATG
per	Sense	CTCAACGCGGGTTAA**T**CA**T**TAACCAAGGAAATG
mut	Sense	CTCAACGCGGG**GC**AACT**G**TGACCAAGGAAATG
Primers used for quantitative PCR		
mUrat1	Forward	GAGGGAGACACGTTGACCAT
	Reverse	AAGTCCACAATCCCGATGAG
mGapdh	Forward	AACGACCCCTTCATTGAC
	Reverse	TCCACGACATACTCAGCAC
Primers used for bisulfite PCR		
mUrat1		
−419-B-F	Forward	GGGAATTAATAAGGGAGTGTAGGAA
+134-B-R	Reverse	TCACCATAAAACCTAAAACCCTCT

EMSA, electrophoretic mobility shift assay.

Results

Involvement of HNF1α/β in the Promoter Activity of *URAT1* Genes. A previous report suggested the presence of *cis*-elements required for the basal promoter activity of the *hURAT1* gene in the region from −253 to −39 base pairs relative to the transcriptional start site (Li et al., 2004). The minimal promoter construct of *hURAT1* was transfected into three human-derived cell lines, and luciferase activities were measured. The *hURAT1* promoter showed a significant increase in luciferase activity compared with the promoterless pGL3-Basic plasmid in HepG2 and Caco-2 cells, whereas the promoter activity was negligible in HEK293 cells (Fig. 2A).

To investigate the involvement of HNF1α or HNF1β in the *hURAT1* minimal promoter, the HNF1 motif found in the *hURAT1* promoter was disrupted by site-directed mutagenesis, and the promoter activity was measured in HepG2 and Caco-2 cells in which endogenous HNF1α and/or HNF1β is expressed (Kikuchi et al., 2006). Mutation in the HNF1 motif completely abolished the promoter activity in both cell lines (Fig. 2B). Direct confirmation of the importance of HNF1α or HNF1β for the promoter activity of *URAT1* genes was obtained by cotransfection assays in HEK293 cells in which neither HNF1α nor HNF1β is endogenously expressed (Fig. 2C). Exogenous expression of HNF1α and/or HNF1β markedly increased luciferase activity of the *hURAT1* wild-type reporter (−253/+83-HNF1wt) compared with the pcDNA3.1(+)-transfected control, whereas the luciferase activity of pGL3-Basic was unaffected. The luciferase activity driven by *hURAT1* HNF1-

mutated reporter (−253/+83-HNF1mut) was not transactivated by exogenously expressed HNF1α and/or HNF1β to the same degree as that of the wild-type construct as expected. The activity of *mUrat1* promoter (mUrat1_−261/+80) was also stimulated by forced expression of HNF1α and/or HNF1β. These results strongly suggest that the minimal promoter activity of human and mouse *URAT1* genes predominantly depends on the function of HNF1α or HNF1β.

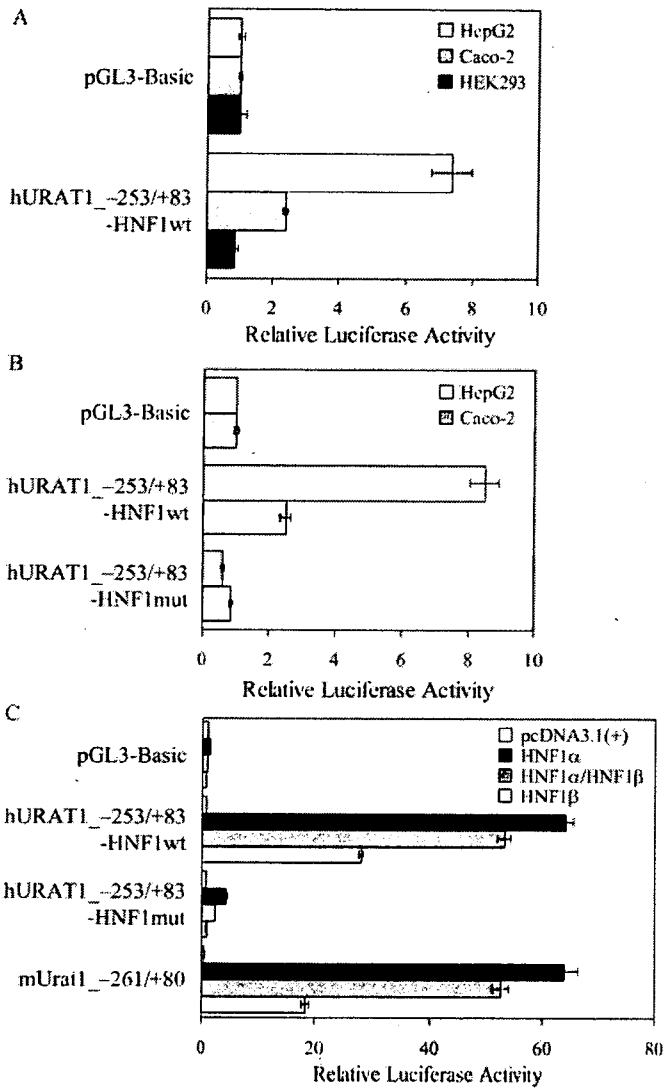

Fig. 2. HNF1α and HNF1β predominantly regulate *URAT1* promoters. A, analysis of *hURAT1* minimal promoter. HepG2 (□), Caco-2 (▨), and HEK293 cells (■) were transiently transfected with promoterless pGL3-Basic plasmid or minimal promoter construct of *hURAT1* (hURAT1_−253/+83-HNF1wt) together with the internal standard pRL-SV40 to normalize the transfection efficiency. B, mutational analysis of the HNF1 motif. HepG2 (□) and Caco-2 cells (▨) were transfected with pGL3-Basic, wild-type (hURAT1_−253/+83-HNF1wt), or HNF1-mutated (hURAT1_−253/+83-HNF1mut) promoter construct. C, exogenous expression of HNF1α and HNF1β. HEK293 cells were transfected with pGL3-Basic, wild-type, or the HNF1-mutated promoter construct of *hURAT1* (hURAT1_−253/+83-HNF1wt or hURAT1_−253/+83-HNF1mut, respectively), or the *mUrat1* promoter construct (mUrat1_−261/+80), together with empty pcDNA3.1(+) vector (white bars), HNF1α expression vector (black bars), HNF1α and HNF1β expression vectors (gray bars), or HNF1β expression vector (light gray bars). The promoter activity was measured as described under *Materials and Methods* and was shown as the induction factor over the background activity measured in cells transfected with pGL3-Basic in each cell line (A and B) or cells transfected with pGL3-Basic together with pcDNA3.1(+) (C). All results are presented as the mean ± S.E. of triplicate samples.

Interaction of HNF1α/β with the *hURAT1* Promoter. Interaction of digoxigenin-labeled oligonucleotide probes (wt, per, and mut) with nuclear proteins of HepG2, Caco-2, or HEK293 cells was assessed by electrophoretic mobility shift assays. The wt probe corresponds to the wild-type HNF1 motif in the *hURAT1* promoter, and the per probe corresponds to the consensus sequence for the HNF1 motif, whereas the mut probe has the same mutation in the HNF1 motif as that used in the luciferase assays. A nonspecific band, which was formed with every probe and abolished by 25-fold molar excess of both per and mut competitor, was observed in all cell lines. In the competition assays (Fig. 3A), one (band *a*) or two shifted bands (bands *a* and *b*) were formed with nuclear extracts derived from HepG2 or Caco-2 cells, respectively, when the wt and per probe were used (lanes 1, 4, 6, and 9). The bands *a* and *b* were abolished by an excess of unlabeled per but not by mut oligonucleotide (lanes 2, 3, 7, and 8), and these bands were not formed when the mut probe was used (lanes 5 and 10). These results suggest that bands *a* and *b* represent the binding of HNF1α or HNF1β to the HNF1 motif in the *hURAT1* promoter. In contrast, there were no specific bands in HEK293 cells (lanes 11 and 12), consistent with the lack of HNF1α and HNF1β in this cell line.

Supershift analysis with antibodies against HNF1α or HNF1β revealed specific interaction of HNF1α and/or HNF1β with the HNF1 motif in the *hURAT1* promoter (Fig. 3B). Addition of an anti-HNF1α antibody supershifted band *a* in HepG2 cells (lanes 3 and 4) and bands *a* and *b* in Caco-2 cells (lanes 8 and 9). Addition of an anti-HNF1β antibody resulted in the supershift of band *b* in Caco-2 cells (lanes 10 and 11), whereas band *a* was not supershifted (lanes 5, 6, 10, and 11). These results suggest that the bands *a* and *b* reflect the binding of HNF1α/HNF1α homodimer and HNF1α/HNF1β heterodimer, respectively. Binding of exogenously expressed HNF1α or HNF1β to the HNF1 motif was also demonstrated. Another shifted band showing faster mobility than HNF1α/HNF1β heterodimer was detected when the nuclear extracts of HEK293 cells transfected with HNF1β alone were incubated with the labeled probe, and this band was supershifted by anti-HNF1β antibody but not by anti-HNF1α antibody (data not shown). This result suggests that HNF1β/HNF1β homodimer can also interact with the HNF1 motif in the *hURAT1* promoter.

Impaired Expression of mUrat1 in *Hnf1α*-Null Mice. Real-time PCR analysis revealed that the expression of mUrat1 mRNA in the kidney is much lower in *Hnf1α*-null mice compared with wild-type mice of both genders (Fig. 4). In contrast to a previous report (Hosoyamada et al., 2004), there was no significant difference in the expression level of mUrat1 between male and female wild-type mice. On the other hand, the expression of mUrat1 mRNA in male mice was significantly higher than that in female in *Hnf1α*-null mice. The difference in *Hnf1α*-dependent expression (wild-type minus *Hnf1α*-null mice) between male and female mice did not reach statistical significance.

Epigenetic Regulation of the *mUrat1* Gene. Eight CpG dinucleotides, primary targets of DNA methylation in the vertebrate genome, are located in the 5′-flanking sequence up to −500 base pairs of *mUrat1* gene; seven of them

are within the minimal promoter region (Fig. 1). To elucidate the role of DNA methylation in the tissue-specific expression of the *mUrat1* gene, the methylation status of each CpG site was analyzed by sodium bisulfite genomic sequencing in the liver, kidney cortex, and kidney medulla, and the total methylation profiles in these tissues were compared (Fig. 5). These CpGs were heavily methylated in the liver and kidney medulla, in which there is no expression of mUrat1. In contrast, the region was relatively hypomethylated in the kidney cortex, in which mUrat1 is predominantly expressed. These results suggest that tissue-specific expression of *mUrat1* gene is regulated through DNA methylation-mediated gene silencing, and the proximal promoter region of the *mUrat1* gene can be regarded as a tissue-dependent differentially methylated region (T-DMR).

Discussion

In the present study, the involvement of both genetic and epigenetic mechanisms in the transcriptional regulation of human and mouse *URAT1* genes was demonstrated. A pivotal role for HNF1α and HNF1β in the minimal promoter activity of *URAT1* genes was confirmed by reporter gene assays (Fig. 2), and interaction of HNF1α/HNF1α homodimer, HNF1α/HNF1β heterodimer, and HNF1β/HNF1β homodimer with the HNF1 motif in the *hURAT1* promoter was shown by electrophoretic mobility shift assays (Fig. 3).

In the kidney, HNF1α normally exists as a heterodimer with HNF1β, although the HNF1α/HNF1α homodimer is a more potent transactivator than the heterodimer in vitro. HNF1β/HNF1β homodimer is also detectable in nuclear extracts from kidney, but the transactivation potency is the lowest among the three species (Rey-Campos et al., 1991; Pontoglio et al., 1996). Because expression of HNF1α is confined to the proximal tubules whereas that of HNF1β is observed along the entire nephron (Lazzaro et al., 1992; Pontoglio et al., 1996), formation of HNF1α/HNF1β heterodimer will be restricted to the proximal tubules in the kidney, and that of HNF1β/HNF1β homodimer is possible in the entire nephron. The expression of human and mouse *URAT1* genes is predominantly in the proximal tubules (Enomoto et al., 2002; Hosoyamada et al., 2004), which is consistent with the distribution of the HNF1α/HNF1β heterodimer. This suggests that the HNF1α/HNF1β heterodimer is required for constitutive expression of human and mouse URAT1. In contrast, the contribution of HNF1β/HNF1β homodimer is debatable. Although the HNF1β/HNF1β homodimer can also transactivate the *mUrat1* promoter, the expression of mUrat1 was markedly reduced in the kidney of *Hnf1α*-null mice (Fig. 4). This supports an essential role for the HNF1α/HNF1β heterodimer, which could not be compensated for by the HNF1β/HNF1β homodimer.

Eight CpG dinucleotides in the 5′-flanking region of the *mUrat1* gene appeared hypermethylated in the liver and kidney medulla, whereas they were relatively hypomethylated in the kidney cortex (Fig. 5). Two mechanisms are proposed for DNA methylation-dependent gene silencing: 1) DNA methylation directly interrupts the binding of transcription factors to their recognition sequences, including the CpG dinucleotide; and 2) methyl CpG binding proteins bound to the methylated cytosine recruit chromatin remodeling factors, such as histone deacetylases, and cause the neighboring chromatin configuration to condense, thereby preventing many transcription factors from accessing their recognition sequences within that region (Shiota, 2004). The HNF1 motif in the *mUrat1* promoter is located within the T-DMR, but the motif itself does not contain the CpG dinucleotide. It is possible that methylation of DNA in the T-DMR indirectly inhibits the binding of HNF1α or HNF1β to the promoter through chromatin remodeling events. Hypermethylation of the T-DMR may explain the absence of mUrat1 expression regardless of the formation of HNF1α/HNF1α homodimers in the liver. In the kidney, the promoter region is hypomethylated in the cortex but hypermethylated in the medulla. Together with the proximal tubule-restricted distribution of the HNF1α/HNF1β heterodimer, the regional difference in the methylation status seems to lead to the constitutive expression of mUrat1 in the proximal tubules in the cortex. In humans, the methylation profiles of *hURAT1* promoter re-

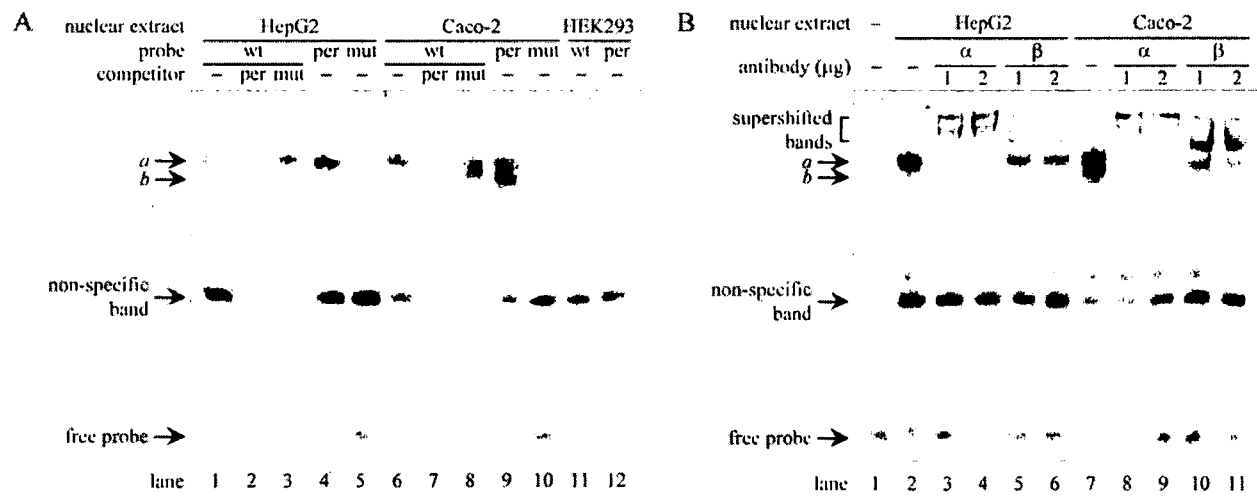

Fig. 3. HNF1α and HNF1β interact with the *hURAT1* promoter. A, competition assays. Three kinds of digoxigenin-labeled probe (Table 1) were incubated with nuclear extracts of HepG2, Caco-2, or HEK293 cells, with or without a 25-fold excess of unlabeled competitor (per or mut) as indicated. B, supershift assays. The wt probe was incubated with nuclear extracts of HepG2 or Caco-2 cells with or without an increasing amount of specific antibody against HNF1α (α) or HNF1β (β) as indicated. The DNA-protein complex was detected as described under *Materials and Methods*.

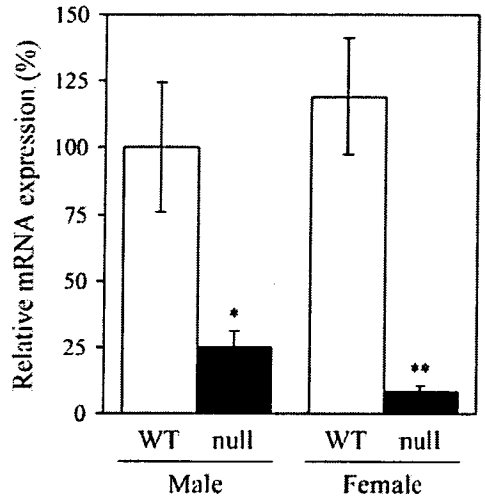

Fig. 4. Relative mRNA expression of mUrat1 in wild-type and *Hnf1α*-null mice. mRNA expression of mUrat1 in the kidneys of male or female wild-type (WT, □) and *Hnf1α*-null mice (null, ■) was measured by real-time quantitative PCR using specific primers (Table 1), and the data were normalized by the mRNA expression of Gapdh. The relative mRNA expression was given as a ratio with respect to the mRNA expression of mUrat1 in male wild-type mice that was taken as 100%. Results are presented as the mean ± S.E. of three (male) or four (female) mice. *, $P < 0.05$, and **, $P < 0.01$, significantly different between wild-type and *Hnf1α*-null mice.

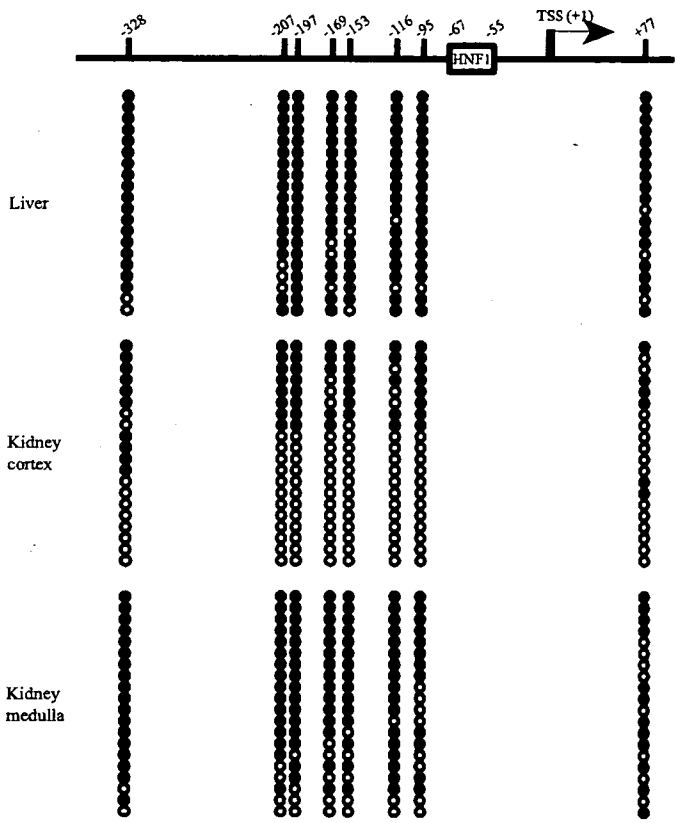

Fig. 5. DNA methylation profile of the *mUrat1* promoter. Top, a schematic diagram of the *mUrat1* 5′-flanking region. The vertical lines and numbers indicate the positions of cytosine residues of CpGs relative to the transcriptional start site (TSS, +1). The position of the HNF1 motif is shown by a rectangle. Bottom, DNA methylation status of individual CpGs. Bisulfite sequencing analysis was performed with genomic DNAs extracted from mouse liver, kidney cortex, and kidney medulla. ○ and ● represent unmethylated and methylated cytosines, respectively.

main unknown. Considering the similar frequency of CpG dinucleotides in the minimal promoter region between human and mouse (Fig. 1), DNA methylation will be also involved in the tissue/region-specific expression of hURAT1.

Mice lacking HNF1α suffer from severe renal Fanconi syndrome, a dysfunction in renal proximal tubular reabsorption (Pontoglio et al., 1996). The renal fractional excretion of urate is higher in mutant animals compared with wild-type controls, resulting in a lower serum urate level. In the present study, in vitro and in vivo evidence of the importance of HNF1α in the expression of *URAT1* genes was provided; accurate tissue-specific expression of this gene is essential for the reabsorption of filtered urate in the kidney. The altered renal excretion of urate in mutant mice is thus accounted for by impaired expression of Urat1. It was reported that expression of transporters responsible for reabsorption of filtered glucose, phosphate, and bile acids is also absent or lower in *Hnf1α*-null mice (Pontoglio et al., 2000; Shih et al., 2001; Cheret et al., 2002). Taken together, the expression of transporters required for the reabsorption of filtered solutes in the kidney proximal tubules is largely impaired in mutant mice, leading to renal Fanconi syndrome.

In addition to renal Fanconi syndrome, *Hnf1α*-null mice exhibit a phenotype similar to non–insulin-dependent diabetes mellitus (Lee et al., 1998; Pontoglio et al., 1998). In humans, mutations in HNF1α and HNF1β cause maturity-onset diabetes of the young (MODY) types 3 and 5, respectively (Yamagata et al., 1996; Horikawa et al., 1997). MODY is an autosomal dominant inherited disease that is responsible for 2 to 5% of non–insulin-dependent diabetes mellitus (Ledermann, 1995), and MODY3 accounts for 20 to 75% of patients with MODY, whereas MODY5 is a rare condition (Froguel and Velho, 1999; Winter and Silverstein, 2000; Ryffel, 2001). It was reported that the serum urate levels are low in patients with both type I and type II diabetes mellitus because of the elevated renal clearance (Shichiri et al., 1987; Magoula et al., 1991; Golik et al., 1993). The increase in the urate clearance has been ascribed to an elevated glomerular filtration rate and/or a defect in tubular urate reabsorption. It is thus possible that the expression of URAT1 mRNA is reduced in patients with MODY3 and MODY5, resulting in hypouricemia.

In conclusion, clear evidence is provided for the involvement of both genetic (HNF1α and HNF1β) and epigenetic (DNA methylation) mechanisms in establishing the tissue-specific expression of mouse and probably human *URAT1* genes. This is the first demonstration of the presence of T-DMR in the promoter region as far as transporters in the kidney are concerned.

Acknowledgments

We thank Dr. Shun Sato for his technical assistance and helpful discussions.

References

Bird A (2002) DNA methylation patterns and epigenetic memory. *Genes Dev* 16:6–21.

Blumenfeld M, Maury M, Chouard T, Yaniv M, and Condamine H (1991) Hepatic nuclear factor 1 (HNF1) shows a wider distribution than products of its known target genes in developing mouse. *Development* 113:589–599.

Cheret C, Doyen A, Yaniv M, and Pontoglio M (2002) Hepatocyte nuclear factor 1 alpha controls renal expression of the Npt1-Npt4 anionic transporter locus. *J Mol Biol* 322:929–941.

De Simone V, De Magistris L, Lazzaro D, Gerstner J, Monaci P, Nicosia A, and